BENCHMARKING OF CRADLE CFD SOFTWARE TO PREDICT STORE SEPARATION TRAJECTORY USING EGLIN TEST MODEL AND THE PREDICTION OF ONSET OF FLUTTER AND THE TRANSONIC DIP USING BSCW WING

By

NUZA NIGAR

500079890

SCHOOL OF ENGINEERING

(DEPARTMENT OF AEROSPACE ENGINEERING)

SUBMITTED

IN PARTIAL FULFILLMENT OF THE REQUIREMENT OF THE

DEGREE OF

MASTER OF TECHNOLOGY

TO

UNIVERSITY OF PETROLEUM AND ENERGY STUDIES

DEHRADUN

(May 2022)

UNDER THE GUIDANCE OF

Dr. Rajesh Yadav

Assistant Professor

UPES

Dr. Karthik Sundarraj

Technical Advisor

Hexagon MI, India

ACKNOWLEDGEMENT

I would like to thank my mentor **Dr. Rajesh Yadav (Associate Professor UPES)**, for constantly supporting me through the project and helping me understand the concept behind certain physics involved. I would also like to thank my external mentor **Dr. Karthik Sundarraj (Technical Advisor, MI India)** for allowing me to intern in Hexagon and work on such projects. I would like to sincerely thank **Mr. Hatazawa Sukujiro (Senior Manager, Sales and Dealer Management, Hexagon Japan)**, for providing me an opportunity to work with him on the flutter prediction case. His constant guidance has helped me prepare to overcome challenges in the project. I would like to thank **Mr. Jonas Wirgart (Product Marketing Manager, Hexagon)**, for his constant guidance throughout my internship. I would like to express warm gratitude to **Mr. Ganesh Pawar R** and **Mr. Praphul T. (Technical Consultants, Hexagon India)** for being such wonderful teammates and supporting and guiding me throughout the work. Without them, this would have been very challenging. I would like to thank **Ms. Katsumura Yumiko (Senior Application Engineer, Hexagon Japan)**, for always being ready to help with any challenges I faced with the software. I would like to express my sincere gratitude to **Mr. Pawel Chwalowski (Aeroelasticity, NASA Langley Research Center)**, for allowing us to work with the AePW III High Angle Working group and giving suggestions on how to improve the results. Also, I would like to thank my course coordinator, **Dr. Gurunadh Velidi**, for always supporting me and guiding me throughout my post-graduation. I will always be grateful to my university, the **University of Petroleum and Energy Studies, Dehradun** for providing me with such platforms to explore the best in me. Last, but not least, I would like to thank my family and friends for constantly motivating me to be the best version of myself.

DECLARATION

I hereby declare that this submission is my own work and that, to the best of my knowledge and belief, it contains no material previously published or written by another person nor material which has been accepted for the award of any other degree or diploma of the university or other institute of higher learning, except where due acknowledgements has been made in the text.

Signature/Name/Date

THESIS CORRECTION CERTIFICATE

This is to certify that the thesis entitled “Benchmarking Of Cradle CFD Software To Predict Store Separation Trajectory Using Eglin Test Model And The Prediction Of Onset Of Flutter And The Transonic Dip Using BSCW Wing” is being submitted by Ms. Nuza Nigar in fulfillment for the Award of MASTER OF TECHNOLOGY in Computational Fluid Dynamics to the University of Petroleum and Energy Studies. Thesis has been corrected as per the evaluation reports dated dd/mm/yyyy and all the necessary changes / modifications have been inserted/incorporated in the thesis.

Signature of Supervisor
Name of Supervisor
Department
Designation
Contact address:
Date:

THESIS COMPLETION CERTIFICATE

This is to certify that the thesis on “Benchmarking Of Cradle CFD Software To Predict Store Separation Trajectory Using Eglin Test Model And The Prediction Of Onset Of Flutter And The Transonic Dip Using BSCW Wing” by Ms. Nuza Nigar in Partial completion of the requirements for the award of the Master of Technology (Engineering) is an original work carried out by her under our joint supervision and guidance. It is certified that the work has not been submitted anywhere else for the award of any other diploma or degree of this or any other University.

Internal Supervisor <Name & signatures>
Name of Supervisor
Department
Designation
Contact address

External Supervisor<Name & signatures>
Name of Supervisor
Department
Designation
Contact address

ABSTRACT

This thesis focuses on the benchmarking of the Cradle CFD software. It also involves the use the MSC Nastran which is the flagship software of Hexagon. The key feature, the computational methodology and the applications of Cradle CFD is highlighted here. The two cases performed are the "Prediction of Store Separation of the Eglin Test Model" and the "Prediction of the onset of flutter and Transonic Dip using the BSCW Wing". The first case highlights the scFLOW features like the overset mesh and the 6 DOF conditions and their ease of use. The second case highlights the Fluid Structure Interaction happening through two way coupling using scFLOW and Nastran. MSC CoSim provides the platform for the cosimulation to occur. Both the cases give results that have a good match with the reference data.

Table of Contents

LIST OF FIGURES

LIST OF TABLES

LIST OF SYMBOLS

Symbol	Variable name	Units
β	Thermal expansion coefficient	$[\frac{1}{K}]$
ϵ	Turbulence dissipation rate	$[\frac{m^2}{s^3}]$
μ	Viscosity ($\mu_i + \mu_t$: molecular viscosity + eddy viscosity)	$[\frac{kg}{m \cdot s} = Pa \cdot s]$
ρ	Density of a fluid or a solid	$[\frac{kg}{m^3}]$
σ_{ij}	Stress tensor	

	$(= \mu\left(\frac{\partial u_i}{\partial x_j} + \frac{\partial u_j}{\partial x_i}\right) - \left(p + \frac{2}{3}\mu\frac{\partial u_k}{\partial x_k}\right)\delta_{ij})$	
d	Source of diffusive terms	$[\frac{1}{s}]$
g_i	Gravity	$[\frac{m}{s^2}]$
i	Dimension ($i = 1, 2, 3$)	
k	Turbulence kinetic energy	$[\frac{m^2}{s^2}]$
p	Pressure of a fluid	N/m^2
$\dot{q}$	Heat Source	$[\frac{J}{m^3 \cdot s}]$
t	Time	$[s]$
u_i	Velocity of flow in $x_i$direction	$[\frac{m}{s}]$
x_i	Coordinates	$[m]$
C	Concentration of diffusive species	$[1]$
C_p	Specific heat at constant pressure	$[\frac{J}{Kg \cdot K}]$
D_m	Diffusion coefficient	$[\frac{m^2}{s}]$
H	Specific enthalpy	$[\frac{J}{Kg}]$
K	Thermal conductivity	$[\frac{J}{m \cdot s \cdot K}]$
R	Gas constant	$[\frac{J}{Kg \cdot K}]$
T	Temperature of a fluid or a solid	$[K]$
T_0	Reference temperature of a fluid	$[K]$

ABBREVIATIONS

Abbreviation	Full form
CFD	Computational Fluid Dynamics
DSO	Defence Science Organization
NASA	National Aeronautics and Science Administration
CTS	Captive Trajectory System
DOF	Degree of Freedom
CAD	Computer-Aided Design
HPC	High Performance Computing
IBVP	Initial Boundary Value Problem
MPI	Message Passing Interface
I/O	Input/Output
FE	Fatal Error
NACA	National Advisory Committee for Aeronautics
BSCW	Benchmark Super Critical Wing
OTT	Oscillating Turn Table
PAPA	Pitch and Plunge Apparatus
N-S	Navier-Stokes
ALE	Arbitratry Lagrangian-Eulerian
CSM	Computational Structural Mechanics
RDF	Radial Basis Function
LDC	Linear Displacement Combination

Chapter 1: Introduction

Hexagon develops the technology based on simulation software that makes a path for the engineers and researchers to validate their product designs and makes way for the optimization of the design. Clients from various industries use the software of Hexagon to complement and sometimes even replace their testing of the physical prototype that traditionally has been there to decide the product design. Hexagon Flagship software MSC Nastran based on Computational Structural Mechanics and Software Cradle CFD based on Computational Fluid Dynamics has occupied major industries like Aerospace, Automotive, Electrical, Life Science, Civil, Marine Technology, and Co-simulation. This project is based on benchmarking the software in the Aerospace and Defence Industry. The first project involves the study and prediction of trajectories in store separation in a transonic regime which is the client-based project of DSO National Laboratories, Singapore. The second project is based on Prediction of Flutter Boundary using the Benchmark Supercritical Wing which is for the Aeroelastic Prediction Workshop III by NASA. [1]

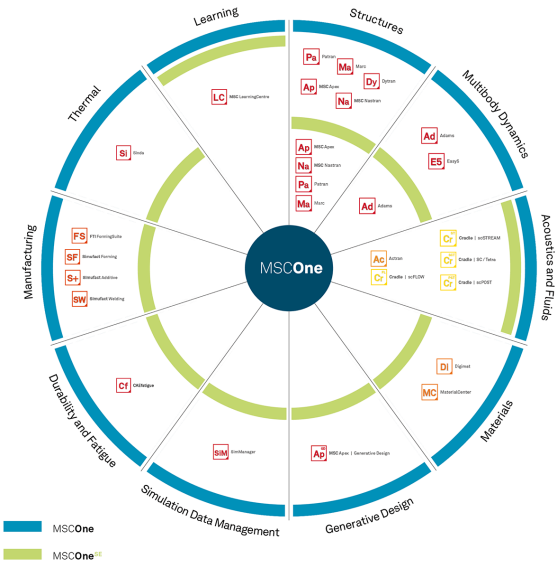

1.1. Predicting the Store Separation Trajectory using Eglin Test Model

1.1.1. Purpose and Objective

The separation of the store from air vehicle is a critical issue in terms of the missile integration process. Store separation tests are expensive, time consuming and dangerous since tests can end up with fatal accidents. Whenever store separates from the aircraft during flight it is extremely required that it does not come in contact with aircraft.[2] Traditionally, flight tests were being performed to test the store separation, however, they were very time consuming and often required years to certify a projectile.[3] In 1960s, Wind Tunnel Testing was done to perform the store separation tests. However, such testing had long lead times and had limited accuracy. The method used in such wind tunnel was the Captive Trajectory System. However, the CTS system had no accuracy in time. Thus, they do not account for the inherent unsteadiness encountered by the store during separation. Also, due to use of small-scaled models, scaling problems often lead to the reduction in accuracy.[4] Development of High Parallel Computing and numerical algorithms has paved a safe path to numerical solutions of Store Separation. Such numerical modelling and simulations have reduced the certification cost and the increased the margin of safety of flight test. Trajectories of stores released from internal weapons bays have been shown in recent tests to diverge from predicted paths. It is critical to develop an accurate method of predicting the trajectory for a transonic regime especially. In transonic regime, a complex transient interaction phenomenon exists, which when must be simulated, needs to consider the compressibility effects and the strong interference flow fields that are generated between the wing and pylon and the store body. In the transonic regime, CFD plays a role of detecting potentially dangerous shock configurations and is part of the system of clearance for flight test and store integration.[5] The simulation of aerodynamically driven, moving-body problems, such as store separation, manoeuvring aircraft, and flapping-wing flight are important goals for CFD practitioners. [6] However, the challenge of CFD is to provide accurate data in timely manner. The computation cost increases due to the use of fine unstructured grids and also

the use of small-time steps to achieve accuracy and stability. Aerodynamic and physical parameters affect store separation problems. Aerodynamic parameters are the store shape and stability, the velocity, attitude, load factor, configuration of the aircraft and flow field surrounding the store. Physical parameters include store geometric characteristics, center of gravity position, ejector locations and impulses and bomb rack. The above parameters are highly coupled and react with each other in a most complicated manner. [7]–[9]. Accurate Prediction of the flow field is necessary for the accuracy in trajectory prediction. The resulting moments and forces as well as the accurate integration of the Equations of Motions is need for prediction. To establish this, the coupling of 6 DOF equations with the Navier Stokes equations is needed.[10] The force and moments on a store can be calculated using CFD applied to the wing, pylon and the store geometry. The purpose of this project is to use Software Cradle to validate the store separation trajectory using the Eglin Test Model. [11]This work also presents a detailed attention to the ejector force profile. The transonic Mach number for which the simulation is performed is 0.95. [12]

1.1.2. Method

The software Cradle's scFLOW code is used to solve the Reynolds Averaged Navier Stokes Equation which is coupled with the 6 Degree of Freedom Equation. The overset meshing technique is used to create the component and the background mesh. The background mesh is created around the wing and the pylon. The component mesh is created around the store. scFLOW uses octree creation to produce the polyhedral mesh with prism layers around the walls. The steady state solution is utilised to proceed with the Time Accurate simulation. The values of the ejector force profile and the moment of inertia is specified within the 6 DOF conditions.

1.2. Prediction of the Onset of Flutter Boundary and Transonic Dip using the Benchmark Supercritical Wing

1.2.1. Purpose and Objective

Fluttering is a common aeroelastic phenomenon. The lowest airspeed at which the structure will oscillate with sustained simple harmonic motion is defined as the flutter speed. [13] When there is positive feedback between the structural deflection and the force exerted by the fluid flow, an elastic structure in a fluid flow experiences dynamic instability. When flutter occurs, the force of fluid acts as a negative damping to the structural vibration, resulting in a continuous increase in vibration magnitude. [14] Aircraft operating at speeds greater than flutter speeds experience a divergent unstable structural oscillation. [14] This project looks at the prediction of flutter onset at 5 degrees of attack angle. It is relevant to the third Aeroelastic Prediction Workshop. [15]

Objectives of Aeroelastic Prediction Workshop: High Angle Working Group[13]

- Predictive use of cutting-edge coupled CFD tools (coupled: structural dynamics and unsteady aerodynamics).
- Apply to configuration and test conditions that push the modeling's range of application (i.e., physics are difficult) due to separated flow and dynamically separating flow.

- Define Mach number, angle of attack, and structural dynamic characteristics regions that require different analysis methods, grid resolution and treatment, temporal resolution, and so on.
- Examine the effect of in-tunnel effects, such as juncture flow, on unsteady characteristics such as flutter.

Transonic conditions are particularly difficult for computational tools to handle because strong shocks can cause separated flow. Many methods rely on equations that do not account for separated flow field physics. Flow separation can introduce flutter into a system. The most dangerous transonic flutter cases are those that occur in the transonic dip, where the onset condition (dynamic pressure at which flutter occurs) can change rapidly in terms of Mach number and angle of attack change. The transonic dip points are difficult to calculate and experimentally obtain.

To understand the onset of flutter, analysis is done through the study of limit cycle oscillations. Wing limit cycle oscillations (LCO) have been observed in flight and in wind tunnel experiments on certain modern high-performance aircraft. It's unclear whether the physical mechanism causing this behaviour is a fluid or structural nonlinearity, or both. It has been demonstrated that an aeroelastic theoretical model with only a structural nonlinearity can accurately predict the limit cycle behaviour of a plate-like wing at zero angle of attack at low subsonic flow. In flight, changes in the limit cycle and flutter behaviour have been observed as the angle of attack is varied. This sensitivity to angle of attack has been attributed to fluid nonlinearity.

Despite advances in computational fluid dynamics (CFD) over the past few decades in turbulence modelling, numerical scheme stability, and code effectiveness for large cases, predicting transonic flutter and LCO, and nonlinear aeroelasticity in general, remains a challenge, and research in this area is ongoing.[14]

1.2.2. Method

At flutter conditions, the Benchmark Super-Critical Wing, BSCW, is used in this study. The experiment is carried out at various dynamic pressures and

speeds ranging from Mach 0.7 to Mach 0.85 at Angle of Attack 5 degrees. This project also focuses on capturing the Transonic Dip, which occurs around Mach 0.8, using Hexagon's co-simulation platform. MSC Nastran is used for Computational Structural Mechanics, and Cradle CFD's scFLOW is used for Computational Fluid Dynamics. MSC CoSim, a co-simulation platform provided by MSC Software, allows for explicit Fluid-Structure Interaction.

Chapter 2: Basic CFD Procedure

Computational Fluid Dynamics Analysis is performed in four steps. These include creating the CAD model, discretizing the domain, setting up the physics of the problem and post processing the results. A 3-D model of the structure under analysis must be created, with all details that have no significant impact on the overall results removed, as these details would only increase the amount of computer work required later in the CFD process. To complete this task, any 3-D modelling tool can be used as long as the software can export the model in the appropriate file format.

Following the creation of CAD, discretisation of the domain needs to be performed. Discretisation is important as the number of equations that is solved during analysis will be based on these finite number of points. Following that, the appropriate method for modelling turbulence must be chosen, and boundary conditions, as well as a number of parameters, must be set in order to achieve convergence. Following that, the residuals and relevant results are visualised and analysed.

Chapter 3: Software Used

- For the case study on Prediction of Store Separation Trajectory, the software used in scFLOW which is a code of CRADLE CFD software.
- For the case study on Prediction of Flutter Boundaries, cosimulation was performed, for which the software used are scFLOW for CFD, MSC Nastran for Computational Structural Mechanics and MSC CoSim for the cosimulation.
- Azure Cloud Computing (HPC) was used to run the simulations.

3.1. Computational Fluid Dynamics Software: Cradle CFD (scFLOW)

Cradle CFD is a collection of useful, cutting-edge CFD simulations and visualization software. It has been used to solve thermal and fluid problems in a variety of applications, including Automotive, Aerospace, Electronics, Building and Architecture, Civil Engineering, Fans, Machinery, and Marine developments.[15], [16]Cradle CFD enables any level user to process advanced simulations by incorporating reinforced Multiphysics co-simulation and chained simulation capabilities to achieve couplings with Structural, Acoustic, Electromagnetic, Mechanical, One-Dimensional, Optimization, Thermal Environment, 3D CAD, and other relative analysis tools, as well as award-winning postprocessing features to generate visually powerful simulation graphics.[16]

Cradle CFD consists of several different codes like scFLOW, scSTREAM, HeatDesigner, SC/Tetra, scPOST, and PICLS. The code used for the above projects was scFLOW for setting up the boundary conditions and the generation of mesh. scPOST was used to perform the post-processing of the results.

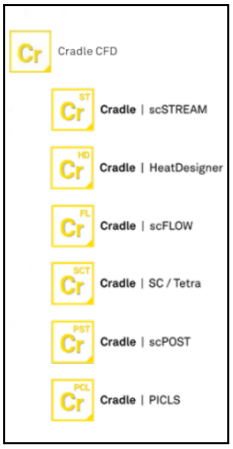

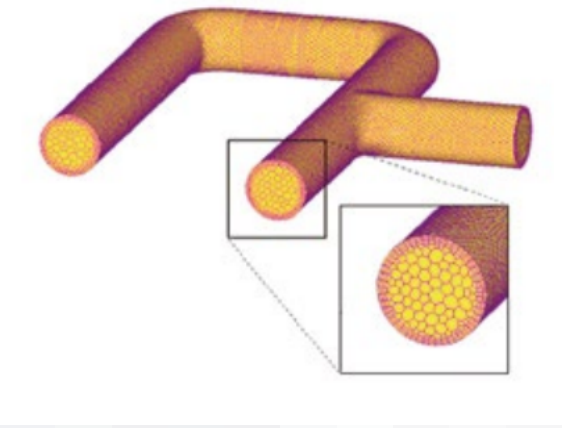

3.1.1. Computational Methodology of scFLOW

The equations used in scFLOW include mass conservation, momentum conservation, energy conservation, turbulent kinetic energy advection and diffusion, turbulent dissipation rate, and diffusive species conservation. [17]

3.1.1.1. The elements and data location of scFLOW

The elements (computational elements) are needed for scFLOW analysis and are used to define the data location in the computational (analysis) region. The data is located at the centroid of each element. The computational region contains as many data points as there are elements. Elements can be shown as the mesh in the two-dimensional view, or rectangular elements can be shown as the 'grid'. The two-dimensional view of arbitrary polyhedrons in scFLOW, on the other hand, does not appear as meshes or 'grids,' so the term element is used.

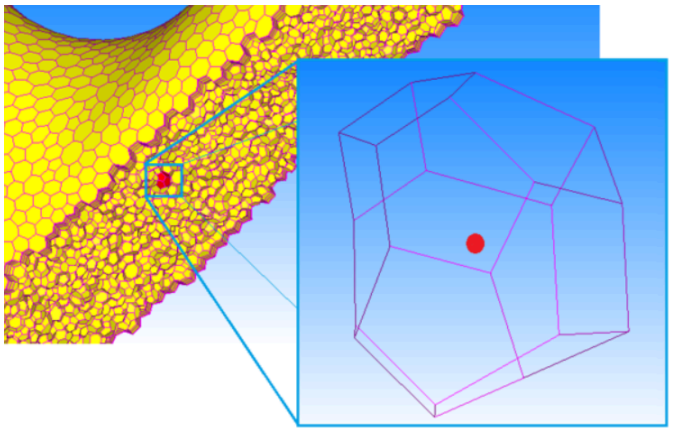

3.1.1.2. Discretization

One of the innovations is to represent the governing equation with discretized data while retaining the characteristics of differentiation. A computer, on the other hand, can only perform arithmetic operations. Unfortunately, a computer cannot directly interpret 'partial differentiation.' All data and equations will be solved using only arithmetic operations, which is why discretization is required. As a method of numerical analysis, the terms 'Finite Element Method' or 'Boundary Element Method' are frequently used. These are also discretization names. The 'Finite Volume Method' is used to discretize scFLOW.[17]

3.1.1.3. The matrix solver

The following matrices form the system of simultaneous equations.

$$\begin{bmatrix} \vdots \\ \phi_i \\ \vdots \end{bmatrix} = \begin{bmatrix} \quad A \quad \end{bmatrix}^{-1} \begin{bmatrix} \vdots \\ S_i \\ \vdots \end{bmatrix} \quad \text{..... Equation 3. SEQ Equation * ARABIC \s 1 1}$$

$$\begin{bmatrix} \quad A \quad \end{bmatrix} \begin{bmatrix} \vdots \\ \phi_i \\ \vdots \end{bmatrix} = \begin{bmatrix} \vdots \\ S_i \\ \vdots \end{bmatrix} \quad \text{..... Equation 3. SEQ Equation * ARABIC \s 1 2}$$

Φi and Si are column vectors, and [A] is a coefficient matrix with phi coefficients as elements. In other words, numerical fluxes are accounted for in [A]. The following equation will be used to solve Φi.

The matrix solver is the numerical procedure used to solve equation 3.1. It is obvious that the matrix solver solves the inverse matrix of [A] in equation 3.2. As a matrix solver, various procedures are proposed, but the iterative method is frequently used due to its flexibility. This is also known as the Krylov subspace method. After assuming an arbitrary Φi, the iterative calculation will be performed with appropriate numerical correction for Φi until Φi approaches the solution. If [A] is a diagonally dominant matrix, the number of iterations

decreases. Before iteration, [A] is reconstructed to be diagonal dominant. This is referred to as a matrix's 'pre-conditioning.'

The iteration schemes based on the conjugate gradient method are used by scFLOW.

3.1.1.4. Pressure correction

The mass conservation shows only spatial variation of flow velocity

$$\frac{\partial u_i}{\partial x_i} = 0$$

$$\rho \frac{\partial u_i}{\partial t} = -\frac{\partial p}{\partial x_i} + F + D + S$$

$$\frac{\partial u_i (\partial p / \partial x_i)}{\partial x_i} = 0$$

Furthermore, the velocity is affected by the spatial gradient of static pressure $\partial p / \partial x_i$. (In the incompressible flow assumption, the time derivative of static pressure in the energy conservation equation is already gone. This is also one of the reasons why three conservation equations are independent)

where, F, D, and S are numerical fluxes and sources except for pressure gradient. When the velocity is solved from equation 3.4 and also satisfies equation 3.3, this velocity is recognized as the correct solution. Hence, velocity should satisfy the equation 3.5.

The pressure correction method refers to the procedure for solving flow velocity based on the spatial pressure gradient. On the assumption of incompressible flow, this method can satisfy both mass and momentum conservation. As a result, the pressure correction method can be referred to as an equation of state for incompressible flows, establishing a link between mass and momentum conservation. When constructing the discretized equation of the momentum conservation equation in the practical computation process, the

relationship of equation 3.5 is taken into account. The iterative method solves the previously mentioned discretized equation while modifying the pressure gradient. The procedure for pressure gradient modification determines the type of pressure correction method.[17]

3.1.1.5. Boundary conditions

Boundary conditions are numerical conditions that must be applied to the computational domain's boundaries. The thermal or flow field is used to select the computational domain as an arbitrary space. Of course, initial conditions and solver algorithms influence analysis results, but assumptions about the computational region's external status also have an impact. Solving the governing equation is an IBVP (initial-boundary value problem) in the mathematical sense. The conditions of the computational region's external statuses are required to solve for the unique result. That defines the boundary conditions.[17]

- Inflow / Outflow conditions
  i. Velocity, Mass Flow Rate, Static Pressure, Total Pressure, and Both Total Pressure and Total Temperature:

     The velocity vector, mass flow rate, temperature, and other parameters can be specified directly for the inflow or outflow boundaries. It should now be noted that the specified values remain constant on the boundary. These constant value specifications are frequently used for inflow and outflow conditions, but it is important to consider whether the boundary value is truly constant. On the inflow boundary from the stagnation region, such as open-air, total pressure and total temperature are frequently used. Only compressible computations have access to the total temperature. It is difficult to apply an exact boundary condition for outflow boundaries; variable status in the computational domain can sometimes generate unwanted partial inflow. To avoid such numerical reverse flows, a computational region may occasionally create an external flow of outflow

boundary. The boundaries of such a region may be specified by the constant static pressure condition.[17]

ii. Natural inflow / outflow:

This is one of the boundary conditions for inflow or outflow, but no constant value is specified. Extrapolation from variables in a computational region near the boundaries will provide the boundary values. This condition most naturally represents the state of boundaries, but incompressible analyses require a constant static pressure boundary on another boundary or pressure fixing on an arbitrary point. Rather, natural inflow/outflow becomes a good flux condition for pressure drop function analyses. a low limit.[17]

iii. Hydrostatic pressure boundary conditions

Gravity is usually taken into account when analyzing a free surface. When gravity is taken into account, high hydrostatic pressure acts on the liquid side. A water surface with a constant water depth, on the other hand, frequently spreads up to inflow/outflow boundaries in an analysis of an open flow, such as flow around a ship. Unnatural flow occurs when a constant static pressure condition is imposed on an inflow/outflow boundary. Because of the pressure difference between the inflow/outflow boundary and the computational domain, this occurs. However, if a natural inflow/outflow condition is specified for such a boundary, reverse flow from an outflow boundary is likely. Hydrostatic pressure boundary conditions can be used to solve the problems.

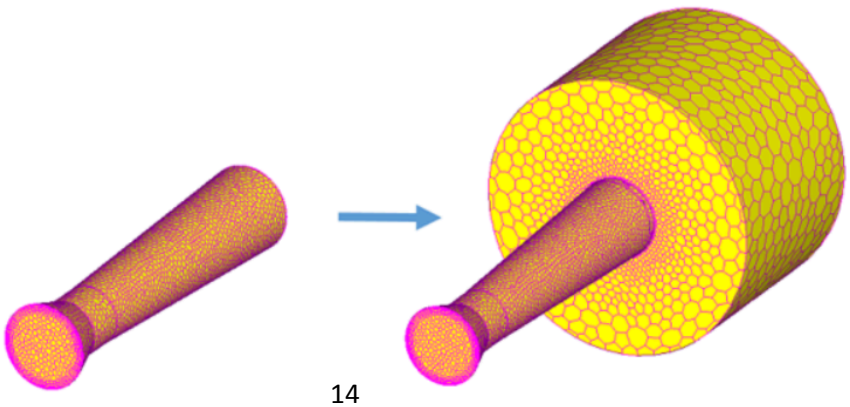

3.1.1.6. Parallel Computing

scFLOW's parallel computing adheres to the MPI (Message Passing Interface) standard. The following is how parallel computing works: The computational domain is first divided into sub-domains. Second, each sub-domain is assigned a process. Third, each process computes its own subdomain while communicating with one another.

Domain partitioning is performed as an internal process by concurrent file I/O, and file I/O always proceeds with the gathered file state. However, if a fatal error (FE error) occurs, error log files are created in each process and the messages are saved. Error messages are also output to the standard output by the rank-0 process.[17]

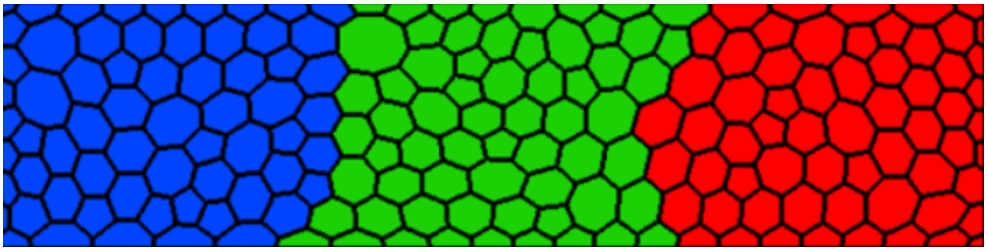

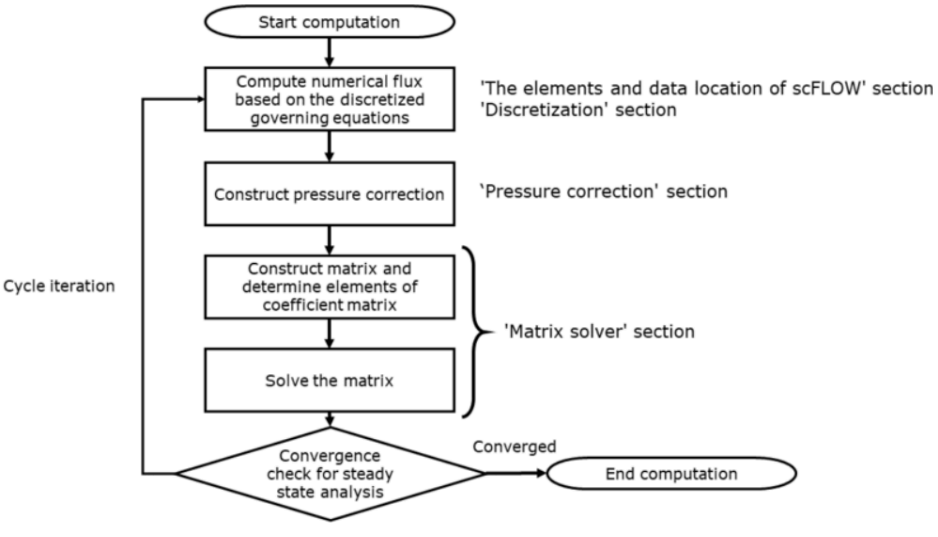

3.2. Computational Structural Mechanics Software: MSC Nastran

MSC Nastran is a general-purpose finite element code that can be used in a variety of disciplines. Linear and nonlinear static analysis, buckling analysis, and dynamic analysis, which include linear, nonlinear, real eigenvalue, complex eigenvalue, direct and modal transient response, and direct and modal frequency response. Heat transfer, sub-structuring, design optimization, composite materials, aeroelasticity, rotor dynamics, and p-element analysis are also supported by MSC Nastran. MSC Nastran's multi-physics solution 400 allows users to perform perturbation studies and coupled thermal structural analysis for advanced analysis. It can also perform combined-analysis types.[18]MSC Nastran is built on advanced numerical methods, the most prominent of which is the Finite Element Method. Nonlinear FE problems can be solved using implicit numerical techniques built into the software.[19]

3.3. Cosimulation Platform: MSC CoSim

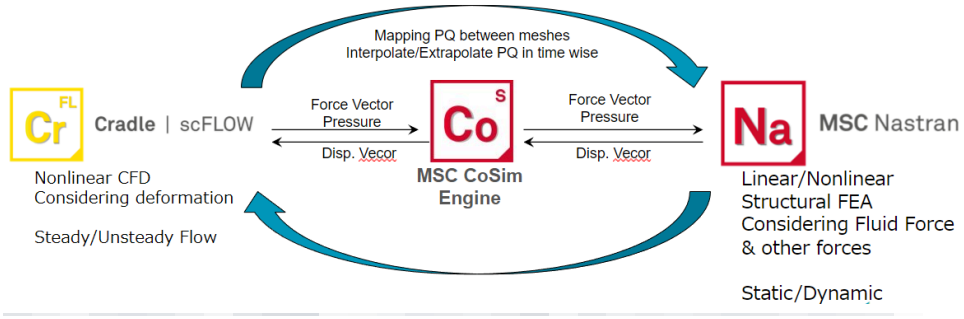

Through the application of MSC CoSim, in this analysis, the flow field and the temperature field from the fluid analysis in scFLOW are mapped to structural mesh as pressure load in MSC Nastran. scFLOW then receives the displacement loads from MSC Nastran and this way two-way coupling is established.

Chapter 4: Resource Limitations

At the time when this thesis was conducted, the fine mesh requirement had to be done with the limit on the amount of RAM available at computing nodes. By use of Azure Cloud Computing, the number of nodes used for computations ranged between 120 – 240 cores. As the number of elements in the mesh increased, the number of nodes increased up to 240 cores in order to reduce the overall computational time.

Table 4.1: HPC execution details

Project Name	Number of Cores	Computation Time	Number of Elements
Predicting the Store Separation Trajectory using Eglin Test Model	240	1 Day (appox.)	2,201,265
Prediction of the Onset of Flutter Boundary using the Benchmark Supercritical Wing	240	2 Days and 3 Hours	422,147

Chapter 5: The Investigated Model under Analysis

5.1. Predicting the Store Separation Trajectory using the Eglin Test Model

The EGLIN test model is made up of three parts that were created using SOLIDWORKS. The first is a delta wing with a constant NACA 64A010 airfoil section and a 45°sweep, the second is a pylon with an ogive-flat plate-ogive cross-section, and the third is a finned store body with an ogive-cylinder-ogive cross-section. The wing's trailing edge has no sweep angle and a taper ratio of 0.133. On the store are four identical fins made of a clipped delta wing of a constant NACA 0008 airfoil section with a 45° sweep. Fins have leading and trailing edge sweep angles of 60 degrees and 0 degrees, respectively. The pylon and the finned body are separated by 35.6 mm. The length and diameter of the store are 3017.5 mm and 508.1 mm, respectively. The store is ejected with enough force to begin a safe initial separation until it falls for 100 mm (the stroke of the ejector piston), after which its motion is subjected to gravity and aerodynamic forces.[20] Table 5.1 shows the store mass, the center of mass position, inertial properties, and ejector parameters

*Table STYLEREF 1 \s 5. SEQ Table * ARABIC \s 1*
1: 6 DOF Properties of the store model[21]

Mass	907.185 kg
Center of Mass	1417.3 mm (aft of STV nose)
Ixx	27.1163 kg-m^2
Iyy	488.0944 kg-m^2
Izz	488.0944 kg-m^2
Forward Ejector Force [F_Z]	10676.0 N
Aft Ejector Force [F_Z]	42703.0 N
Forward Ejector Moment [M_Y]	-1920.0 Nm
Aft Ejector Moment [M_Y]	14057.0 Nm
Ejector Piston stroke length	0.10 m

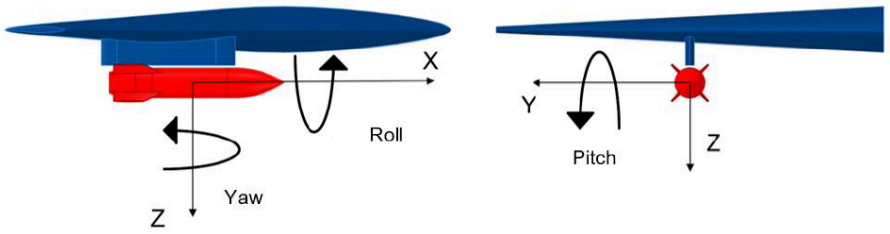
X
Roll
Yaw
Z
Y
Pitch
Z

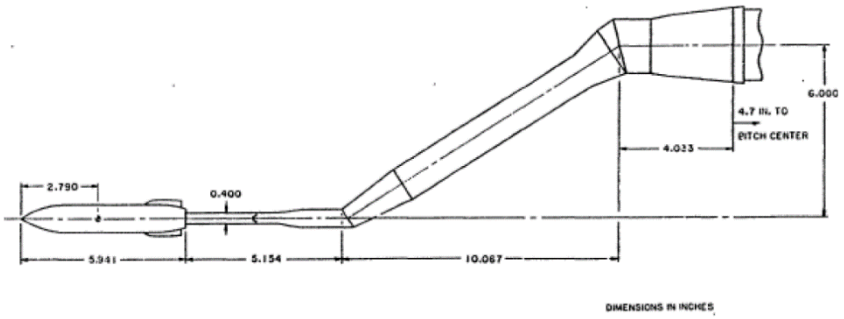
6.000
4.7 IN. TO
PITCH CENTER
4.033
2.790
0.400
5.941
5.154
10.067
DIMENSIONS IN INCHES

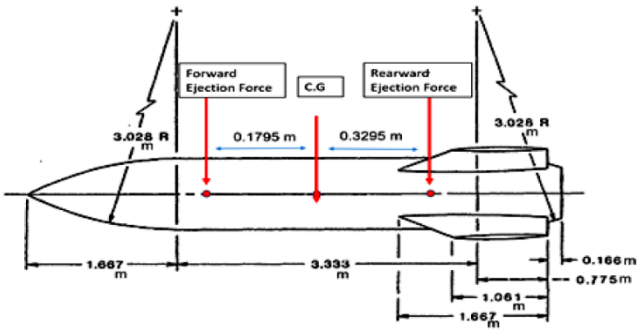
Forward
Ejection Force
C.G
Rearward
Ejection Force
3.028 R
m
0.1795 m
0.3295 m
3.028 R
m
1.667
m
3.333
m
0.166 m
0.775 m
1.061
m
1.667
m

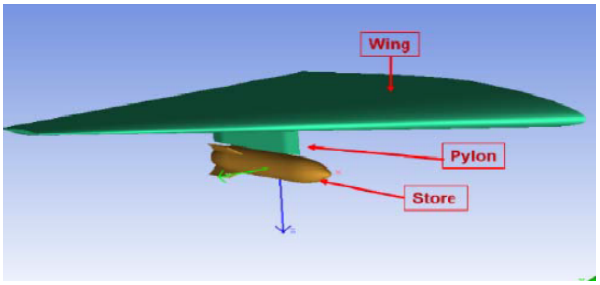
Wing
Pylon
Store

5.2. Prediction of the Onset of Flutter Boundary and Transonic Dip using the Benchmark Supercritical Wing (BSCW)

The NASA Langley Transonic Dynamics Tunnel was used to test the Benchmark Supercritical Wing (BSCW). The most recent test served as the foundation for AePW-1; testing was done on the oscillating turntable (OTT), which provided data on forced pitch oscillations. A previous test on a flexible mount system indicated the pitch and plunge apparatus (PAPA). The model was tested for aeroelastic properties on the PAPA, where the mounting system provides low-frequency flexible modes that simulate a plunge mode and a pitch mode. PAPA data is made up of both steady and unsteady data at flutter points. Data from both tests has been used for comparison.[24]

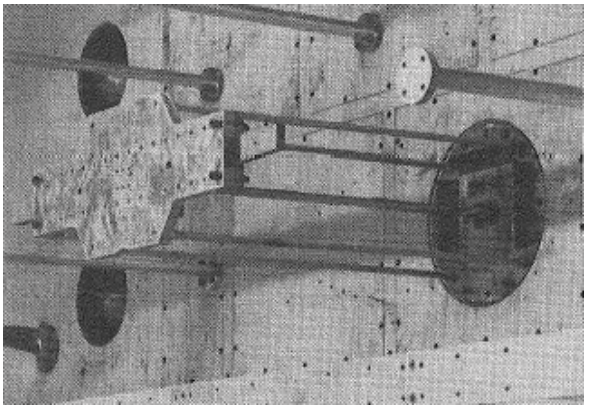

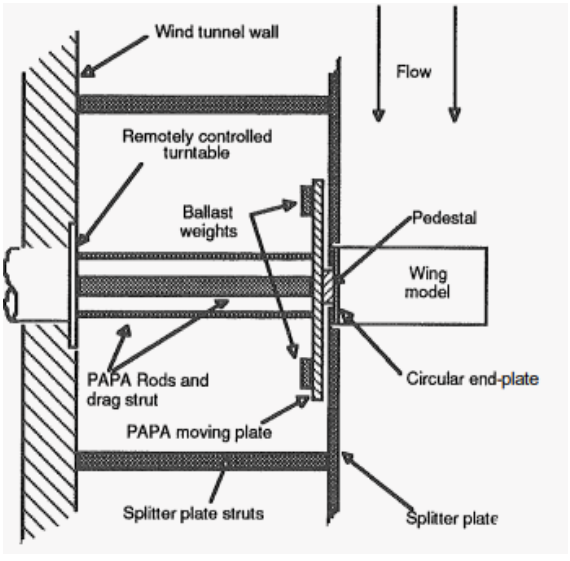

NASA SC(2)-0414 airfoil is used on the BSCW. The airfoil designation indicates that it was designed as part of the second generation of supercritical airfoils, with a design normal force coefficient of 0.4 and a thickness to chord ratio of 14 percent. The planform is rectangular, with wingtip caps shaped like revolution tips. The PAPA test was performed with several flow transition strip configurations; for these comparisons, only data from the 35 grit will be used. The boundary layer transition was set at a 7.5 percent chord for the OTT test using size 30 grit. Transition grit is present on both the upper and lower wing surfaces in all cases.

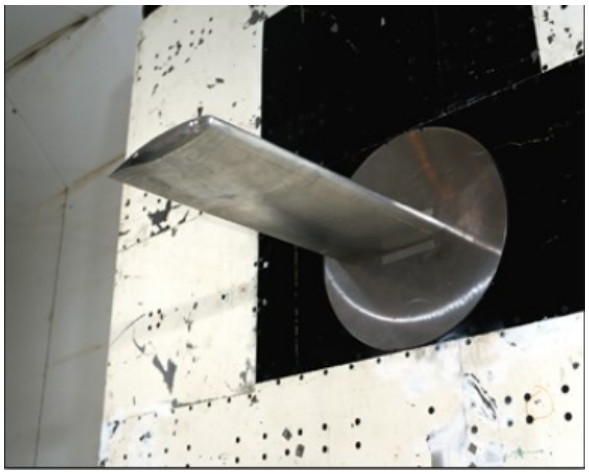

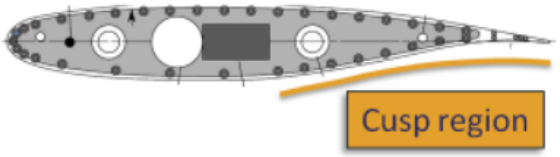

Cross-section at 60% span

Chapter 6: Predicting the Store Separation Trajectory using the Eglin Test Model: Numerics and CFD Process

6.1. Numerics

6.1.1. The Governing Equations

The study is performed by coupling the conservation equations with the 6 DOF equations.

6.1.1.1. *Conservation Equations:*

Solving potential equations, Navier-Stokes (N-S) equations could be at the heart of any CFD application. The N-S relationship describes how pressure, temperature, and density are related to a moving fluid. They consist of a set of coupled partial differential equations; one continuity equation for mass conservation, three equations for momentum conservation, and one equation for energy conservation, all of which are time dependent. Although theoretically possible, these equations are extremely difficult to solve analytically and are thus more commonly solved on computers via approximations. The conservation equations are given as follows.

The equations used in scFLOW include mass conservation, momentum conservation, energy conservation, turbulent kinetic energy advection and diffusion, turbulent dissipation rate, and diffusive species conservation.[17]

Mass Conservation Equation:

$$\frac{\partial \rho}{\partial t} + \frac{\partial}{\partial x_i}\rho u_i = 0$$

$$\frac{\partial \rho}{\partial t} + \frac{\partial}{\partial x_i}\rho u_i = 0$$

$$\frac{\partial \rho H}{\partial t} + \frac{\partial u_j \rho H}{\partial x_j} = \frac{\partial p}{\partial t} + \frac{\partial u_j p}{\partial x_j} + \sigma_{ij}\frac{\partial u_i}{\partial x_j} + \frac{\partial}{\partial x_j}K\frac{\partial T}{\partial x_j} + \dot{q}$$

Momentum Conservation Equation:

$$\frac{\partial \rho u_i}{\partial t} + \frac{\partial u_j \rho u_i}{\partial x_j} = \frac{\partial \sigma_{ij}}{\partial x_j} + \rho g_i$$

$$\frac{\partial \rho u_i}{\partial t} + \frac{\partial u_j \rho u_i}{\partial x_j} = \frac{\partial \sigma_{ij}}{\partial x_j} + \rho g_i$$

Energy Conservation Equation:

$$\frac{\partial \rho H}{\partial t} + \frac{\partial u_j \rho H}{\partial x_j} = \frac{\partial p}{\partial t} + \frac{\partial u_j p}{\partial x_j} + \sigma_{ij}\frac{\partial u_i}{\partial x_j} + \frac{\partial}{\partial x_j} K \frac{\partial T}{\partial x_j} + \dot{q}$$

Equations Of Turbulence Kinetic Energy and Turbulence Dissipation Rate (k-ε equations):

$$\frac{\partial \rho k}{\partial t} + \frac{\partial u_i \rho k}{\partial x_i} = \frac{\partial}{\partial x_i}\left(\frac{\mu_t}{\sigma_k}\frac{\partial k}{\partial x_i}\right) + G_S - G_{S1} - G_{S2} - G_{S3} - \rho\epsilon$$

$$\frac{\partial \rho \epsilon}{\partial t} + \frac{\partial u_i \rho \epsilon}{\partial x_i} = \frac{\partial}{\partial x_i}\left(\frac{\mu_t}{\sigma_S}\frac{\partial \epsilon}{\partial x_i}\right) + C_1\frac{\epsilon}{k}(G_S - G_{S1} - G_{S2} - G_{S3}) - C_2\frac{\rho\epsilon^2}{k}$$

$$\frac{\partial \rho k}{\partial t} + \frac{\partial u_i \rho k}{\partial x_i} = \frac{\partial}{\partial x_i}\left(\frac{\mu_t}{\sigma_k}\frac{\partial k}{\partial x_i}\right) + G_S - G_{S1} - G_{S2} - G_{S3} - \rho\epsilon \quad \frac{\partial \rho \epsilon}{\partial t} + \frac{\partial u_i \rho \epsilon}{\partial x_i} = \frac{\partial}{\partial x_i}\left(\frac{\mu_t}{\sigma_S}\frac{\partial \epsilon}{\partial x_i}\right) + C_1\frac{\epsilon}{k}\left(G_S\right.$$

Diffusive Species Conservation Equation

$$\frac{\partial \rho C}{\partial t} + \frac{\partial u_j \rho C}{\partial x_j} = \frac{\partial}{\partial x_j}\rho D_m \frac{\partial C}{\partial x_j} + \rho \dot{d}$$

Gas equation of state

$$p = \rho R T$$

The equations in "Mass conservation equation", "Momentum conservation equation", "Energy conservation equation", and "Diffusive species conservation equation" are derived by considering the conservation of mass, momentum, energy, and diffusive species in a control volume ‘V’ surrounded by an arbitrary closed surface.

6.1.1.2. Moving Elements: 6 DOF Equations

To simulate flows around moving objects, scFLOW employs the **ALE (Arbitrary Lagrangian-Eulerian) method**,[27] which handles both the moving coordinate system and the fixed coordinate system at the same time. The effect of mesh movement is added to the equation of the fixed coordinate system in the moving region, and the fixed and moving coordinate systems are calculated simultaneously. Moving condition setting for a moving region, as well as selection and setting of the connection method for both static and moving regions, are required in the simultaneous calculation with the ALE method. By applying the moving condition to the volume region containing the object, the moving object is represented. Translation and rotation are examples of settable motions. The static and moving regions can be connected by an overset mesh.[28]

The effects of element motions are incorporated into the equations for the fixed coordinate system in ALE. The following effects are added to the fixed coordinate system's mass conservation equation and momentum equations:[17]

Mass conservation equation

$$\frac{\partial \rho}{\partial t} + \frac{\partial}{\partial x_i}\rho(u_i - v_i) = 0$$

Momentum conservation equations

$$\frac{\partial \rho u_i}{\partial t} + \frac{\partial (u_j - v_j)\rho u_i}{\partial x_j} = \frac{\partial \sigma_{ij}}{\partial x_j} + \rho g_i$$

In the energy conservation and turbulence equations, the advection term (second term on the left side of the equation) must be replaced by $(u_j - v_j)$. The term v_j refers to the mesh's speed of movement. It's worth noting that all of the variables in this section use values from the fixed coordinate system.

For the combination of the moving elements, the complex movement of the object under investigation is simulated using the 6 DOF Motion. The equation of motion can be used to compute the pressure and viscous stress of a fluid, as well as the motion of a rigid body to which an external force is applied. To construct the equation of motion, the mass and moment of inertia[29] of the portion moving as the rigid body are automatically calculated from its material properties. [17]

The 6 DOF solver computes the translational and angular motion of an object's center of gravity using the object's forces and moments. In the inertial coordinate system, the governing equation for the translational motion of the center of gravity is solved.[3]

$$\dot{\vec{v}}_G = \frac{1}{m}\sum \vec{f}_G$$

v_G is the translational motion of the center of gravity, m is the mass, and f_G is the gravitational force vector. Using body coordinates, the angular motion of the object, w_B, is more easily computed:

$$\dot{\bar{\omega}}_B = L^{-1}\left(\sum \bar{M}_B - \bar{\omega}_B \times L\bar{\omega}_B\right)$$

$$\dot{\vec{\omega}}_B = L^{-1}\left(\sum \vec{M}_B - \vec{\omega}_B \times L\vec{\omega}_B\right)$$

Here, where L is the inertia tensor, M_B is the moment vector of the body, and w_B is the rigid body angular velocity vector. The moments are transformed from inertial to body coordinates using Equation 6.1.

$$\bar{M}_B = R\bar{M}_G$$

As a result, the translational equation describes the aircraft in terms of its three translational degrees of freedom, whereas the rotational equation describes the aircraft in terms of its three rotational degrees of freedom. As a result,

Newton's second law yields six equations for the six degrees of freedom of a rigid body. To predict the trajectory of store separation, two sets of equations, Navier-Stokes equations and Equations of motion, must be solved concurrently.

6.1.1.3. Steady-state calculations

The steady-state calculation is performed in the initial stages of the simulation without the use of 6 DOF Equations by having not to use to the moving element conditions. The results of the steady-state simulations are adopted as the initialization for the transient state calculation. For this thesis, the steady-state simulation was run for 2000 cycles.

6.1.1.4. Time accurate calculations

When it is determined that the case under investigation is unsteady in nature, time-accurate computations are used. As mentioned above, the steady-state solution acts as the initialization for the transient state calculation.

6.2. Aspects Regarding the CFD Process

The CFD process for this investigation is described in this chapter. The modelling and discretization processes are covered in the first two subchapters, and the scFLOW process is covered in the final subchapter.

6.2.1. 3D CAD Modelling

The Eglin Test Model consisting of the wing, the pylon, and the store is modelled in SOLIDWORKS software. Added to the model is the external flow domain which is known as the computational domain where the external flow over the model will be analyzed. The size of the computational domain has to be large enough so as not to have any influence on future computations. A cylindrical domain is created on the store which has future needs in the overset meshing. The cuboidal domain is created where one is the near field domain, and the other is the farfield. Size of the farfield domain is (747x347x747) m.

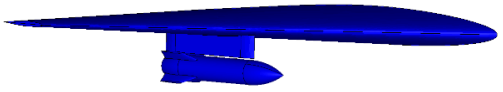

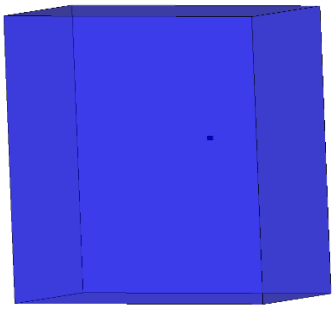

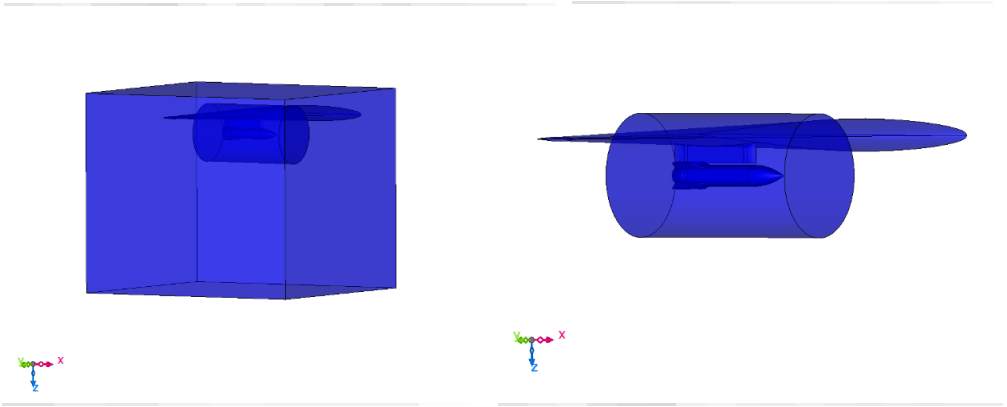

When the geometries are satisfied, scFLOW features the turning on of overset mesh before building the analysis model.

26.2.1.1 Overset Mesh

The overset mesh, in which multiple meshes overlap, can solve moving objects that a discontinuous mesh cannot solve or replace meshes in a portion of the analysis space with another mesh. The overset mesh scheme has three main steps in its process. First, the domain of mesh (elements) to be used for computation is chosen from a set of partially overlapping meshes. Because the domain of mesh that is determined to be unnecessary for the computation is treated as inactive, this process is known as "Hole cutting" (outside of the analysis domain).[17] The list of "acceptor" elements to be used for inter-mesh communication on the cutting surface of the domain determined to be active (inside the analysis domain) and the list of "donor" elements to be used as the opposing side of communication with the acceptor elements are then constructed. These two steps are processed as part of the computation's pre-processing. The main part of the computation connects and solves matrixes of coefficients derived by discretizing the governing equation on each mesh using the list constructed in the second step. When the computation domain contains a moving mesh, the pre-process, i.e. hole cutting and element list construction, is performed at each time step.

For this thesis, the two meshing units that are created in scFLOW are the background unit and the component unit. The background unit consists of the wing and the pylon, whereas the component unit consists of the missile body.

6.2.2. Build Analysis Model

After the CAD Geometry is ready, scFLOW has the feature of building the analysis model out of the CAD. By doing this, a number of facets are created on the model which helps in removing all the unnecessary curved edges that may interfere with the solution. Since there are two components of the overset mesh that consist of the geometry, the build analysis model will be created twice, one for each unit. This group of triangle facets which are created during the build analysis model is used for subsequent mesh generation.

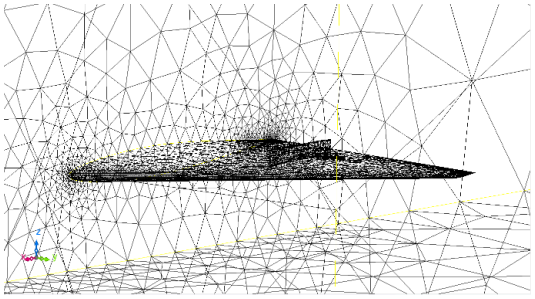

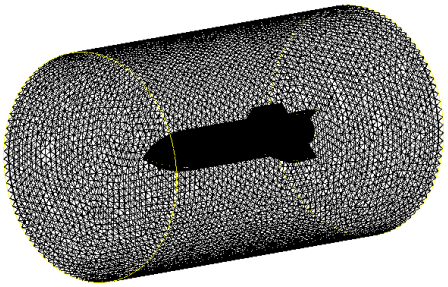

6.2.3. Discretisation

The goal of discretization is to divide the physical space in which the flow is to be computed into a large number of geometric elements called grid cells, within which the governing equations for each element are solved.[30] The various geometric element types available include triangular and quadrilateral elements, which are used in 2-D grids as well as on the surface mesh of a 3-D grid. The other elements shown in Figure 19 are used in 3-D grid volume meshing. Grids are classified into two types: structured grids and unstructured grids. Structured grids are distinguished by regular connectivity, which can be expressed as a two or three-dimensional array, reducing storage requirements and allowing for efficient solver algorithms. Structured grids are limited to quadrilateral elements in the surface mesh and hexahedral elements in the volume. A well-designed structured grid provides an accurate solution; however, creating such a grid is a time-consuming task (and can take months

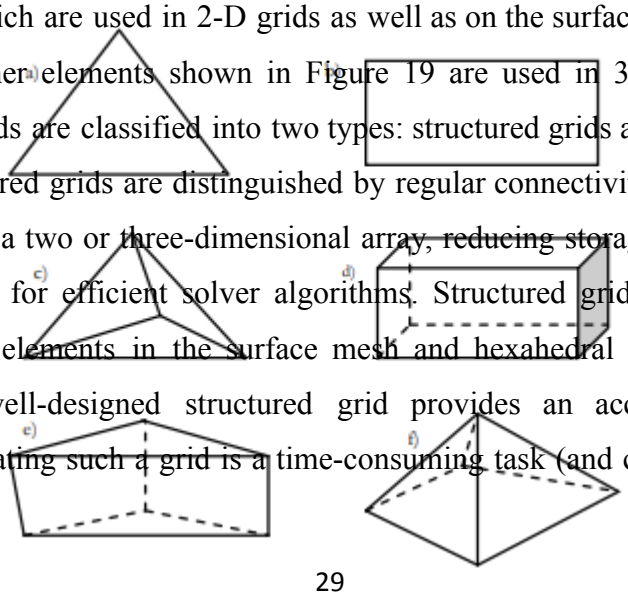

when dealing with complex geometries). Unstructured grids, on the other hand, can include all the elements shown in Figure 19, the grid is referred to as a mixed or hybrid grid. The elements are not ordered and are arranged in an ad hoc manner. This grid is the most used in commercial solvers today. The neighbourhood connectivity of the different cells must be explicitly stored due to the irregularity of the grid distribution, which requires significantly more storage space than for structured grids.

4.2.3.1 Mesh Type in scFLOW

Elements are placed in a region to analyze physical phenomena and calculate changes in physical quantity. scFLOW includes a polyhedral mesher (arbitrary polyhedrons) to improve the cell-centered Solver's stability and calculation accuracy. This is an automatic mesher that will generate mesh based on the number of elements specified, making mesh fine near the wall surface where a rapid flow change is anticipated. Mesh coarseness can also be specified for each part and region. [32] The mesh generation involves the creation of octree and the generation of the polyhedral mesh along with the prism layers which are inserted along the wall. The coarseness of the mesh is specified. However, a finer octree is automatically generated along the walls. The octree size corresponds to the resolution of the result and the reproducibility of the model geometry. As the distance from the wall is uniform by using prism layers, velocity gradient and temperature gradient can be calculated accurately, and

calculation stability is ensured. The calculation time and memory consumption are proportional to the number of elements.

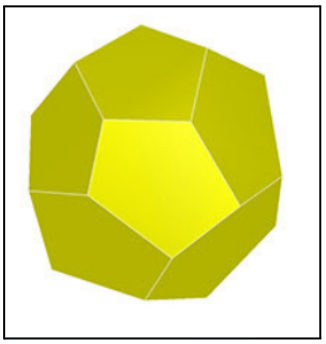

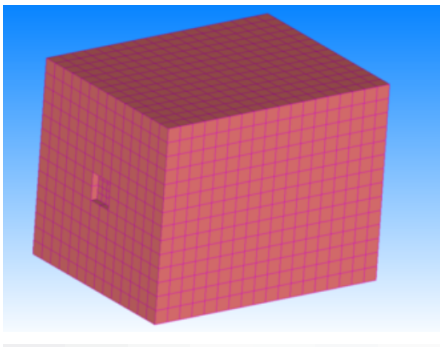

4.2.3.2 General Quality Aspects of a Mesh

When creating a mesh, there are a few things to keep in mind because the quality of the grid influences the end result. A poor-quality grid may have an impact on both numerical stability and accuracy. Naturally, the resolution should be as high as possible, but this consumes more computing resources and results in slower turnaround times. There should be no gaps or overlapping elements in the grid. Furthermore, grid points should be clustered around areas of interest such as regions of high gradient (e.g., boundary layers, separation points, and shocks), pressure changes, and sharp corners or curves. Also, the transition from small to large elements should be smooth so that the volume of the grid cells does not change abruptly. Low-interest areas could have relatively large elements to reduce the total number of elements. There should be no significant kinks in the grid lines of quadrilateral and hexahedral elements when they are present, as this could lead to a significant increase in numerical errors. Finally, the orientation of the cell faces must be checked to ensure that they are normal to the flow gradient.

4.2.3.3 Meshing Method Used

Step 1 Creation of octree

To specify mesh resolution to determine the scale and accuracy of the analysis during mesh generation is of utmost importance. To understand the concept of octants, it is important to know that the size of an octant is

equivalent to the size of the polyhedral element. By referring to the figure, it becomes easier to understand that the root octant gets divided into different levels and subdivided further. Here the root octant is the octant that is larger than the cube that contains the entire domain.

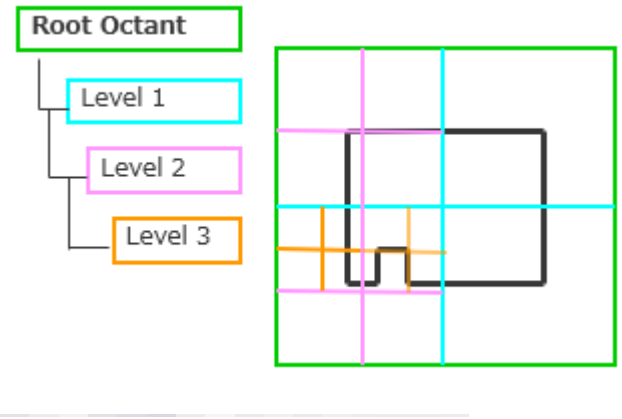

There are three choices that can be made to specify the octant parameter. They are as follows:

- Target a number of elements and let the octree generator decide on the sizes.
- Determine the sizes with a minimum value which will be applied to the surfaces then the octree is coarsened
- Control the octree with detailed parameters (sizes) on surfaces and volumes

For this thesis, the final option is employed. Also, referring to the two units that exist in our project due to the use of the overset mesh, the octree creation also takes place separately for each of these units. For the first meshing unit, the minimum octant size for all the surfaces is given as 12.8 and the maximum octant size is also of the same value. Since there is space in the far-field, octants are coarsened up to this size, which is the maximum octant size. The octant refinement level is specified from the near-wall up to the far-field. For the second meshing unit, the minimum and the maximum octant size are specified as 0.1, for the same reasons stated above. Figures 25 and 26 show octrees for both the meshing units 1 and 2 respectively. The number of

elements generated for meshing units 1 and 2, while creating the octree is 2254965 and 280709 respectively.

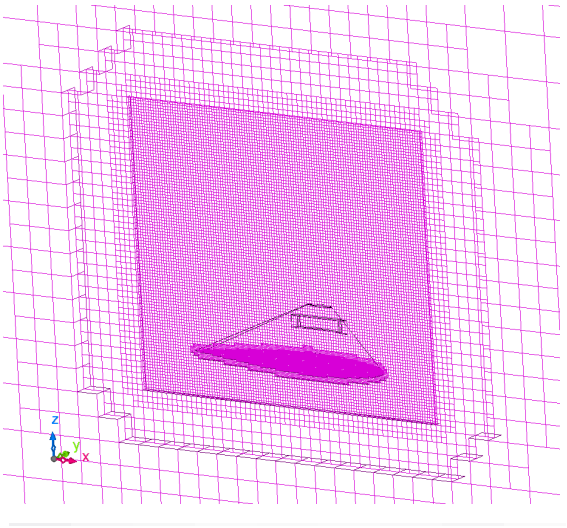

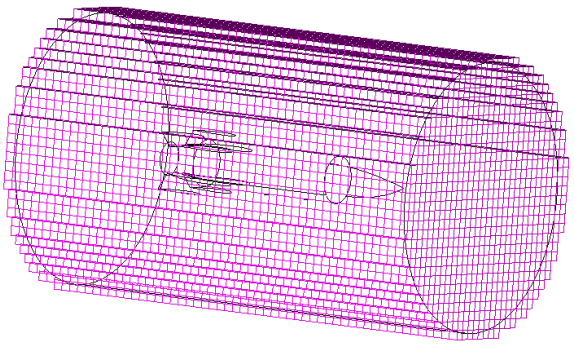

Step 2 Polyhedral Mesh Generation

scFLOW automatically provides the creation of the prism layer along the walls. Since The distance from the wall is not uniform without the prism elements, sufficient accuracy cannot be obtained for velocity and temperature gradient. However, with the prism elements, the distance from the wall

becomes uniform. Sufficient accuracy can be obtained for velocity and temperature gradient as well as the prism layer has the advantage for both calculation accuracy and stability. Here the prism layer is generated along the walls of the wing, the pylon, and the store. Figure 27 and 28 shows the prism layer insertion along the walls.

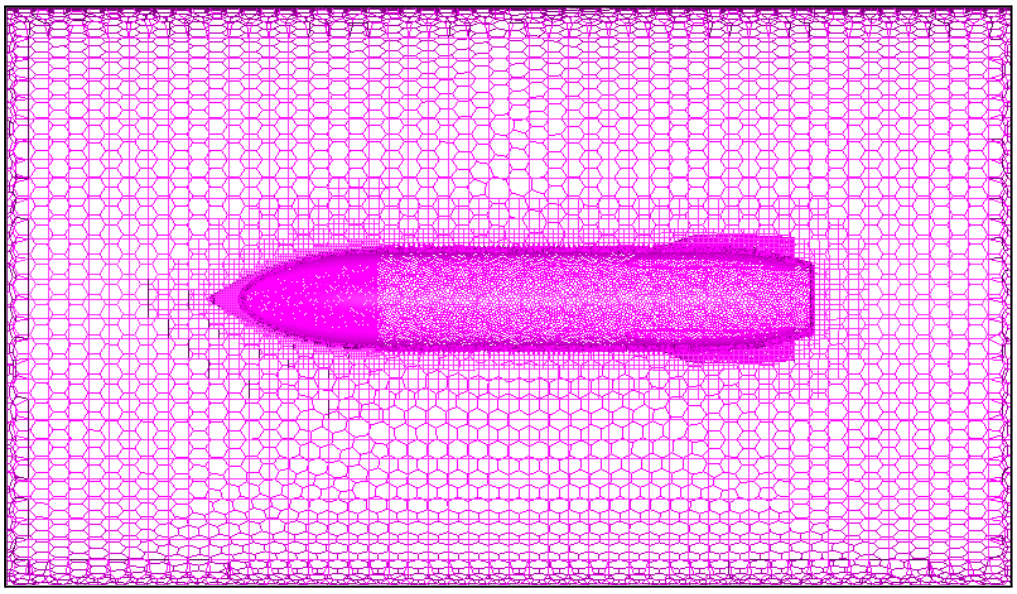

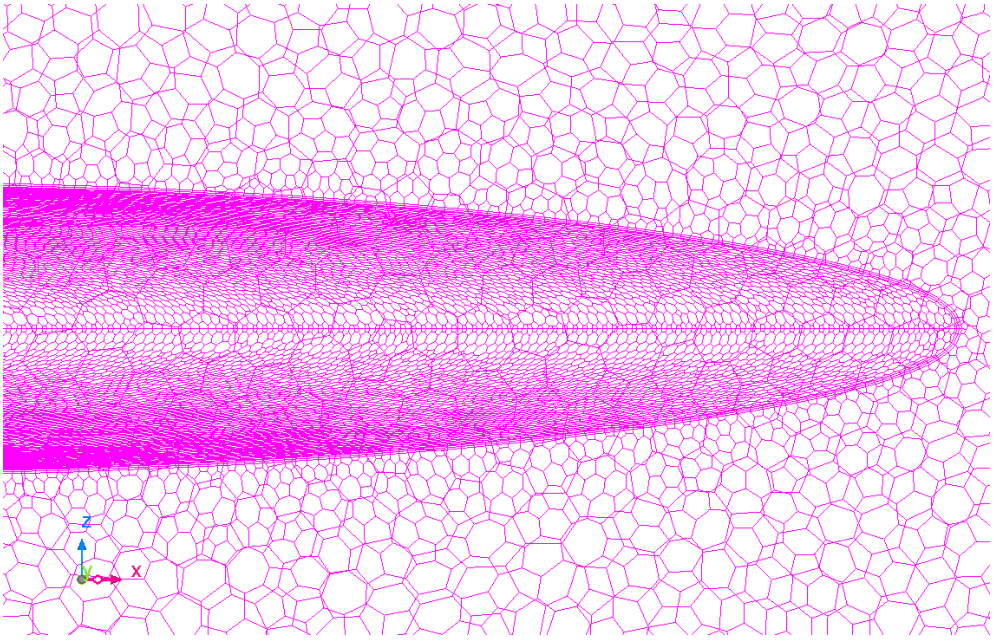

The walls have been modelled as the no-slip boundary wall. For this reason, the insertion of the prism layer elements is highly recommended. The number of prism layers specified here is 2 and the thickness of the prism layer is 0.2. The first layer is calculated automatically by the tool based on the octant size specified on the wall. It can still be captured manually based on the y+ and number of layers required.

As the polyhedral which is an unstructured mesh is generated, the final count of the number of elements is 22,01,265. The element quality is checked by judging the negative volume check. It is ideal that no negative volume element exists because such an element lowers the stability of the analysis. If a negative volume element exists, make the mesh finer or simplify geometry to improve the mesh quality. For this case, zero negative volume check count was found.

6.2.4. CFD Solver Process

6.2.4.1 Material Specification and Registering Regions

The wing pylon body and the missile body are modelled as an obstacle. The fluid around the obstacle is modelled as the compressible air at 20 degrees Celsius.

As it is known that the 6 DOF features is being applied in this problem and the importance to the ejector forces are being given, thus, to apply the ejector force, the forward and the rearward ejector surface needs to be registered. The inlet and the outlet are registered on the boundaries of the computational domain, as well as the symmetry and the $y_{max.}$ For reference to create the points at which the forward and ejector forces are applied, the point of the center of gravity is created. The coordinates of which are as follows:

- Centre of gravity: (1.899, -3.0986, -1.57941)
- Forward Ejector Points: (2.079, -3.0986, -1.57941)
- Backward Ejector Points: (1.57, -3.0986, -1.57941)

6.2.4.2 Analysis Conditions

Since the flow involved in the thesis is a compressible flow, the density-based solver is used. The density-based solver solves simultaneous equations

without breaking them down into conservation equations. Mass conservation solves the mass conservation problem for compressible fluids and is satisfied by rigorously tracking the density change. Because density, pressure, temperature, and velocity are all interdependent, the system of equations can be closed by adding an equation of state to each conservation equation. Because density change always takes precedence over other conditions in a mass conservation problem, this type of solver is referred to as a "density-based solver."[17] It should be noted that flows with less energy influence can be solved without using the energy equation; however, in general, all three conservation equations (mass, momentum, and energy) are solved simultaneously.

According to the preceding concept, the density-based solver is not appropriate for the analysis with slow flow and rapid density change, which is solved smoothly in the pressure-based solver.

The density-based solver is appropriate for compressible fluid analysis with a fast flow and significant energy change. Furthermore, mass conservation solvers tend to be more accurate than pressure-based solvers. Thus, nonlinear waves, such as a shock wave in a fast air current, can be solved stably using the Riemann solver.[33]

The density-based solver is appropriate for transonic (Mach number; around 1) and supersonic fluids. However, using local-preconditioning technology, extremely slow compressible and incompressible analyses can be performed even with the density-based solver. When the pressure-based solver cannot solve it stably, it can be considered as an alternative.

The method of obtaining the in a calculation cycle through the density-based solver is shown in Figure 6.15. Because of the aforementioned solver characteristics, density-based solvers are frequently used for analanalyzingysing high-speed flows.

The time scale of density change or pressure change (propagation time of pressure fluctuation through the fluid) approaches that of flow change in a high-speed flow, and as a result, the effect of compressibility produces some

improvements. A wave motion, such as a shock wave or an expansion wave, appears as one of the effects of compressibility

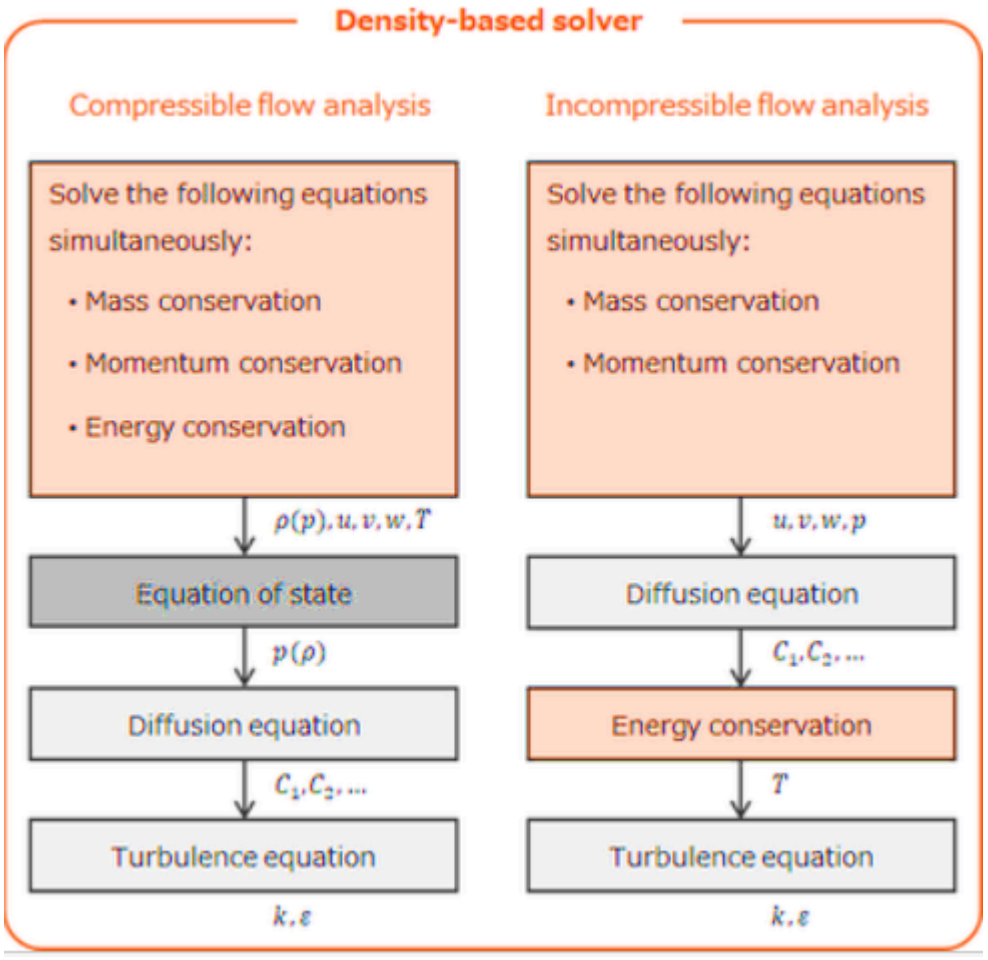

When the pressure or density of a fluid changes in a local area, the change propagates as a wave at the speed of sound. When focusing on a subsonic flow, for example, the wave appears to propagate to the surroundings instantaneously; this may not be considered a flow phenomenon if such wave motion is not a crucial factor. This serves as the foundation for the assumption of incompressibility. When the flow is sonic or supersonic, the impact of the shock wave becomes significant and cannot be ignored. To convey the

changes, three types of waves are used: a shock wave, an expansion wave, and a contact surface. If a flow moves faster than the speed of the wave conveying the changes, the wave is compressed by the flow and becomes steep (the wave's velocity never exceeds the sound velocity), causing some rapid changes in density or pressure. This is referred to as a "shock wave." The expansion wave is the polar opposite of the shock wave, and it expands the medium through which it travels. In compressible flow, a contact surface (also known as a "slip surface" or "shear wave") can be found. The pressure and velocity around the contact surface are stable, but the density changes. [17], [33]

The turbulence model employed for this thesis is the standard k-EPS model. [4], [34] The k-EPS model is the 2-equation closure model which includes two additional transport equations, which are the turbulence kinetic energy k and the turbulence dissipation Epsilon. [35]

$$k = \frac{1}{2}\overline{u_i' u_i'}$$

$$\epsilon = \nu \overline{\frac{\partial u_i'}{\partial x_j} \frac{\partial u_i'}{\partial x_j}}$$

Here, the k-EPS model is employed as it is best suited to study the flow far away from the wall. Since the thesis aims to study the flow changes and the trajectory prediction of the store away from the wall, the k-EPS model is best available to help understand the changes in flow that happen aerodynamically away from the wall of the wing. This consequently affects the store separation taking place.

Since the energy equations are also being solved, the scFLOW pre-processor required the turning on of the Heat analysis type. Further, as we have the inclusion of the 6 DOF equations, the software requires the ‘Moving

Elements' feature to be turned on as well. However, this will only be the case when the transient simulation is done. There is no need to keep the moving element feature on when the steady-state analysis is done to initialize pressure, temperature, and velocity.

Initially, for the initialization of all the parameters of the conservation equation, the steady-state analysis is performed. The steady-state simulation is made to run for the 20000 cycles till the convergence occurs. The default temperature is set at 236.7 K. The gravity is considered in the positive Z direction as the orientation of the model and the base value of pressure is specified equal to the absolute pressure.

Once we get the solutions for the steady-state condition, the .rph file which contains the restart file in scFLOW is used as the initialization for the time-accurate calculations.

For the transient analysis, the time step was taken at 0.0001 and the simulation is run for a total of 0.32 seconds. [12]

6.2.4.3 Boundary Conditions: Flow, Wall, and Symmetry

The number and type of boundary conditions (BC) vary depending on how the physical geometry is constructed. Regardless of which BC is selected, there is usually no need to further edit the BC because the defaults are usually sufficient for all specifications. In scFLOW, there are four types of BCs: flow, wall, thermal, symmetrical, and periodic, each with its own set of BCs. Here, only the wall, the flow, and the symmetrical boundary condition have been applied.

The simulation has been performed in the transonic regime. The Mach number under consideration is 0.95.[12] At the inlet, the velocity component and the Mach number are specified. The velocity component is in the negative X direction as the inlet is registered in the same. The outlet is defined as the Static Pressure (Outflow) where the pressure value is specified as 36042 Pa.

The top, bottom, and y_{max} are defined as the free slip wall boundary condition. The free slip boundary condition is not the same as the no-slip boundary

condition. There is a difference. According to the no-slip boundary condition, both the normal and tangential components of the fluid velocity field are equal to zero at the interface between a moving fluid and a stationary wall. The free-slip boundary condition, on the other hand, states that at the interface of moving fluid and a stationary wall, the normal component of the fluid velocity field is equal to zero, but the tangential component is unrestricted. This condition is also known as the no-penetration condition.

Parameters	Value
Static temperature	236.7 K
Reference Pressure	36042 Pa
Mach No.	0.95
Turbulence model	RANS, k-epsilon
Time-step	1e-04 [s]
No. of elements	2.2 million

The symmetry defined in the negative Y direction is given the symmetrical boundary condition. The boundaries can be clearly seen in the figures given below.

Table 6.1: Analysis conditions Used

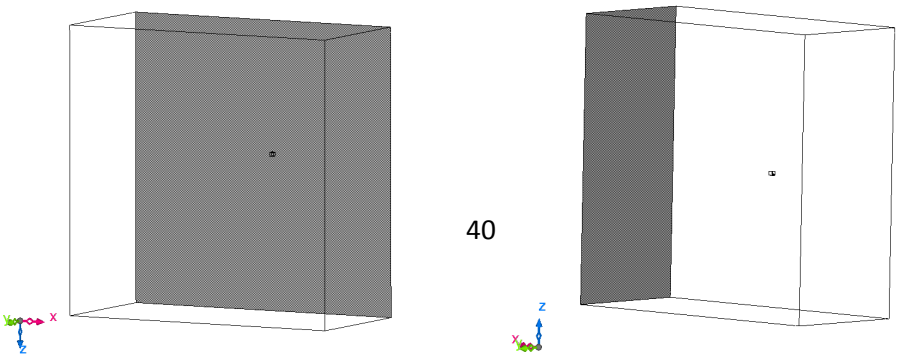

6.16 (a)

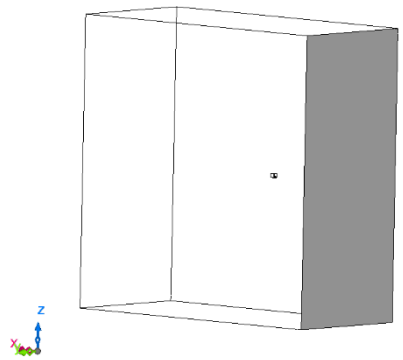

6.16 (b)

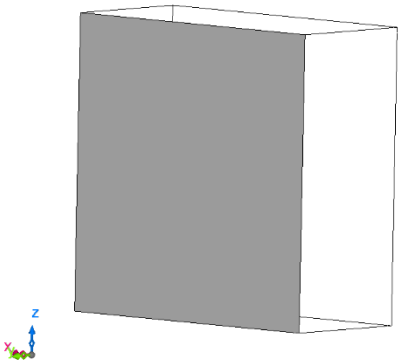

6.16 (c)

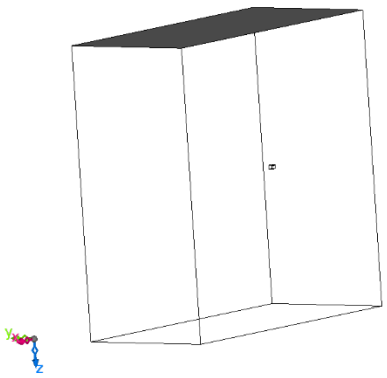

6.16 (d)

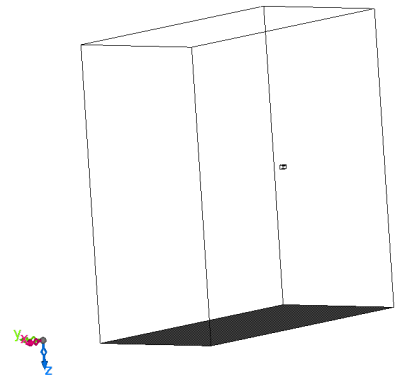

6.16 (e)

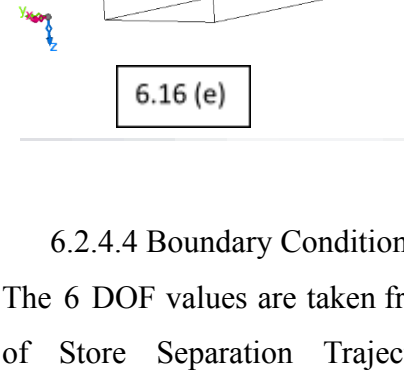

6.16 (f)

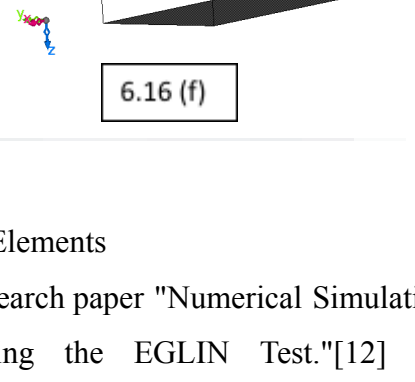

6.2.4.4 Boundary Condition: Moving Elements

The 6 DOF values are taken from the research paper "Numerical Simulations of Store Separation Trajectories Using the EGLIN Test."[12] The computations begin at t=0s to obtain the aerodynamic forces and moments, and then the solver is coupled with a 6-DOF code to predict the entire store

trajectory using the quasi-steady approach. The store is subjected to both forward and aft ejector forces, which are turned off once the ejector stroke lengths are exceeded.The expectation for the results by applying these ejector forces is that for a real-time of t = 0.06 seconds, the store pitches up due to ejector forces acting on it. After the effect of the ejector forces fades, aerodynamic forces acting on the store take control, resulting in a pitch down moment.[36] The 6 DOF Parameters are shown in Table 6.1.

The 6 DOF features are applied to the missile body where the motion type is selected as the 6 Degree of Freedom of Motion of Rigid Bodies. The type of rotation and translation is unrestricted and the surface region for which the force is calculated in the missile body. The mass of the missile body is specified as 907.2 kg. The parameters are specified as given in Table 6.2.

*Table STYLEREF 1 \s 6. SEQ Table * ARABIC \s 1 2: The 6 DOF parameter application in scFLOW*

Parameter	Value	Unit
Centroid		
Coordinate X	1.899	m
Coordinate Y	-3.0986	m
Coordinate Z	-1.57941	m
Moment of inertia	Specify tensor	
A11	27.12	kg· m2
A21	0	kg· m2
A22	488.09	kg· m2
A31	0	kg· m2
A32	0	kg· m2
A33	488.09	kg· m2

The forward and the rearward ejector force is applied in the tabular format according to their working since the ejector forces act for 0.06 s and then stop. The action of the ejector force is shown in the Figures 31 and 32.

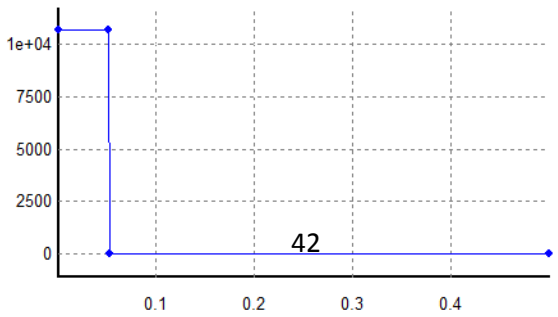

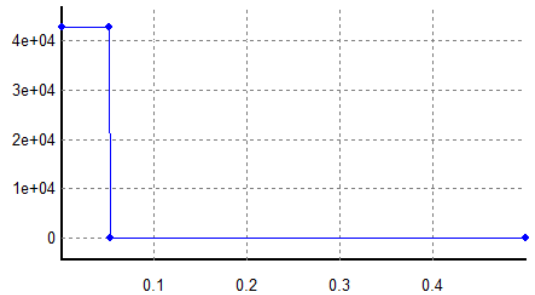

6.2.4.5 Analysis Control Methods

To set the under-relaxation coefficient, for the system of equations of the density-based solver, we specify the value as 0.2. The under-relaxation coefficient for the equations of density-based solver and turbulence and diffusion is set as 0.2,0.7 and 0.99 respectively. Second-order accuracy with limiter is used for the Accuracy of the convective terms for the mass, momentum, energy, turbulence, and the diffusion equation. First Order Accuracy of Time Derivative is used. The least Square is used for Gradient Calculation Method.

6.2.4.6 Output Files

ScFLOW produces a solution in the format of .fph files and L which contains the data and the required variables for analysis, which otherwise remains off by default. The Time series data can also be produced. Here the field file is produced after every 0.01 seconds, and the Mach number is output in the whole domain as Partial Field Files. The Displacement in the x, y, and z directions is output with respect to time.

6.3 Results: Attaining Accuracy through Comparisons and Testing

6.3.1 Linear Displacement versus Time Graph

Figure 33(a-c) depicts the trajectory of the center of gravity locations over time as compared to experimental data. When the store separates from the aircraft due to gravity and ejector forces, it begins to move backward, downward, and inward. After about t=0.2 seconds, the inward and backward movements begin as shown in Figure 35. Vertical displacement appears to match the experimental data very closely. This is due to the fact that the ejector and gravity forces outweigh the aerodynamic forces in this direction. The small difference in horizontal displacement is to be expected because drag is understated due to viscous effects. Overall, the linear displacements in all three directions agree very well with the experimental data.

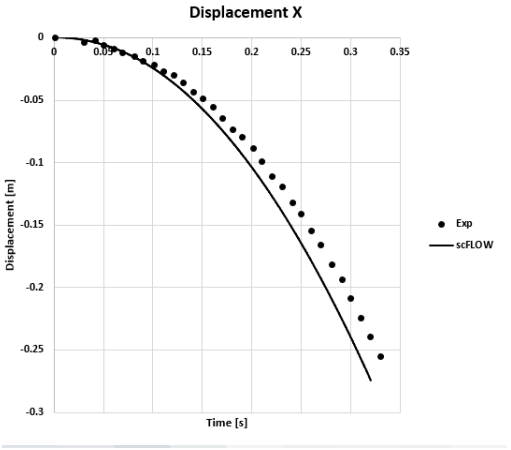

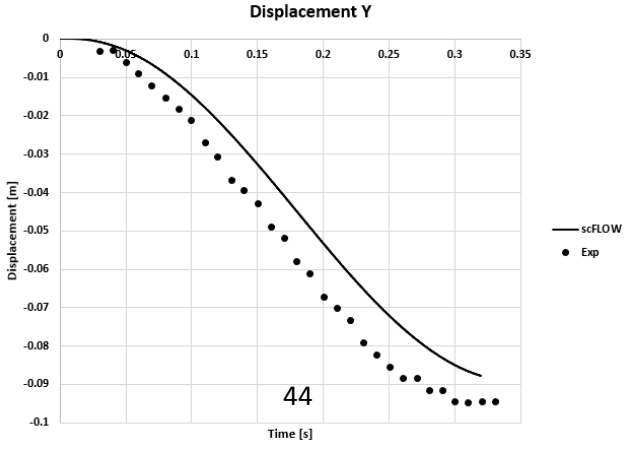

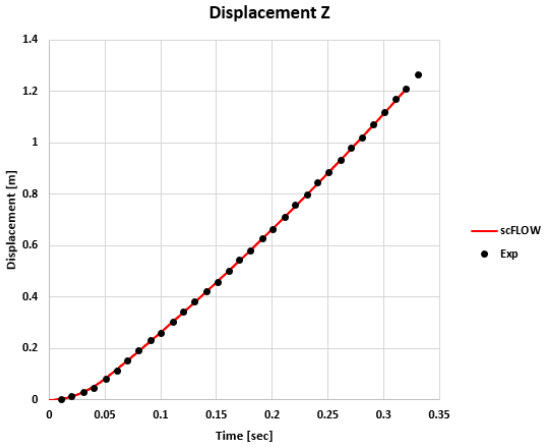

6.3.2 Angular Displacement versus Time Graph

Figure 34 (a-c) compares the trajectory for the center of gravity angular orientations with respect to time to the experimental data. Because of aerodynamic forces, the store moves in a pitch up, yaw, and right roll direction. The ejector forces act on the store until real-time t=0.06 seconds, which is the primary cause of the store pitching up. After being free of the influence of ejector forces, the motion of the store is defined by aerodynamic forces, which is why the store begins to pitch down around t=0.19 seconds.

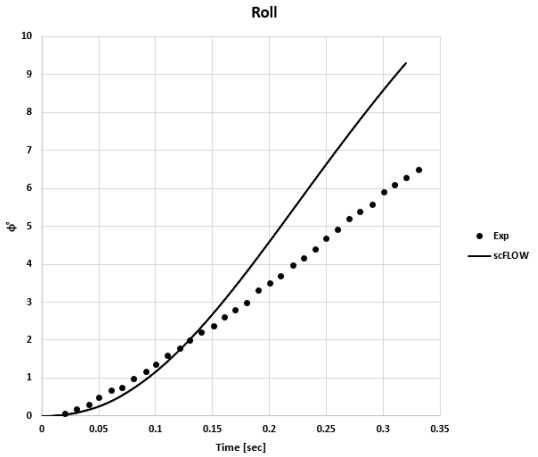

Figure STYLEREF 1 \s 6.22: Angular Displacement vs Time (Roll Orientation)

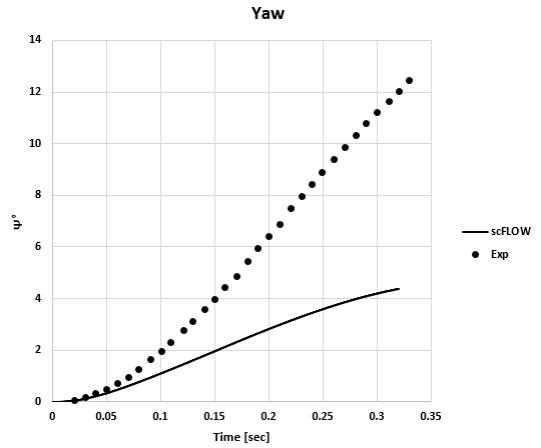

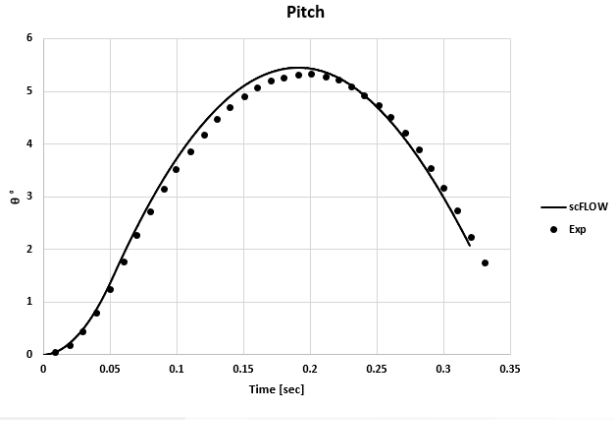

After being separated from the aircraft, the store begins to roll to the right. When compared to the experimental data, the right roll trend is nearly identical. Although the trend is very similar, the results show a minor deviation from the experimental values. The difference in data values begins around 0.052 seconds, just as the ejector forces disappear.

The trend for the yawing moment, which also acts towards the left side of the wing, is similar to experimental data, but there is some

disagreement with the experimental results. This difference grows over time, reaching a maximum at t=0.33 seconds.

6.3.3 Mach Contours

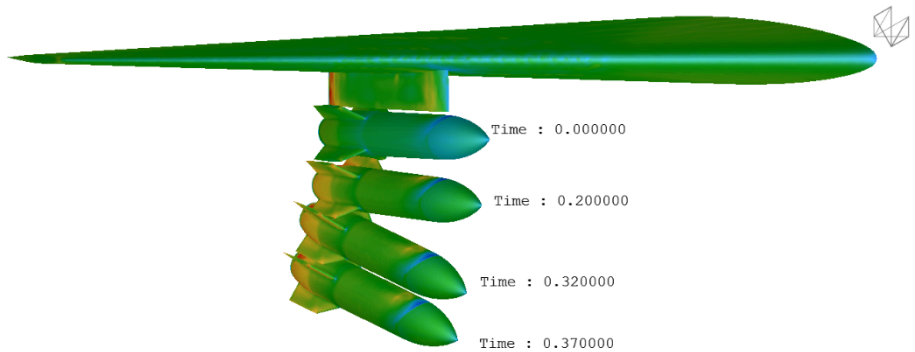

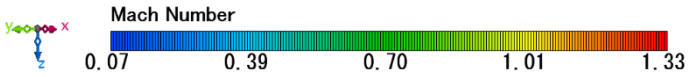

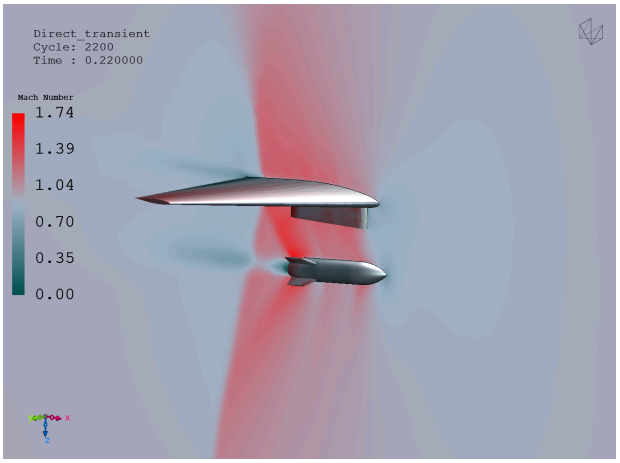

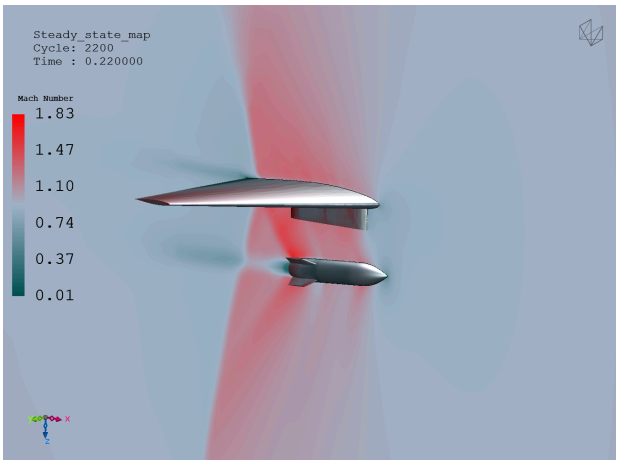

To check if the steady state solution is required in the beginning of the transient simulation, a case was also simulated where the simulation was entirely transient and there was no steady state initialisation for the same. Pressure, Temperature and Velocity is initialized directly in the transient simulation The Mach contours shown in the above figure show that there was not much difference in the shock pattern observed.

6.3.4 Future Work Recommendations

The work on the store separation can be continued forward in many ways. A flexible Eglin case be executed to check for the structural deformations that might occur in the wing due to the weight of the missile body. Also further, accuracy can be improved while predicting the trajectory of separation by either refining the mesh or performing a deep study concerning the time step used. The same separation case can be executed using a different wing model like the Common Research Model prepared by NASA. Also, this case of store separation can be combined with the other case on Flutter mentioned in this thesis to check if the flutter phenomenon has any drastic consequences on store separation.

Chapter 7: Prediction of the Onset of Flutter Boundary and Transonic Dip using the Benchmark Supercritical Wing: Numerics and CFD Process

7.1 Numerics

7.1.1 The Governing Equations

The governing equations here involves the equations based on Computational Fluid Dynamics which is the Navier Stokes Equation and the equations based on Computational Structural Mechanics which is differential non-linear equation valid for a dynamic system with large displacements

7.1.1.1 Computational Fluid Dynamics Equations

The conservation equations solved by scFLOW during this analysis is the same as given by Equation 6.1 – 6.6. It solves the Navier Stokes Equation based on Finite Volume Method.

7.1.1.2 Computational Structural Mechanics Equations

The CSM solver uses a differential non-linear equation valid for a dynamic system with large displacements based on Finite Element Method. The Nastran file is defined to model the structural shape, mesh, thickness distribution of the shell elements, material, and displacement constraint. The governing equations for the CSM analysis are given by Equation 7.1 – 7.5

The equation of motion of a structure is given by Equation 7.1

$$Ma + Cv + Ku = F \quad \text{.....Equation STYLEREF 1 \s 7. SEQ Equation * ARABIC \s 1 1}$$

To solve the equation of motion of a dynamic system, generalized alpha method is used as direct integration, which is given by Equation 7.2

$$Ma^{n+1+a_m} + Cv^{n+1+a_f} + Ku^{n+1+a_f} = F^{n+1+a_f} \quad \text{Equation STYLEREF 1 \s 7. SEQ Equation * ARABIC \s 1 2}$$

where,

$$\text{.....Equation STYLEREF 1 \s 7. SEQ Equation * ARABIC \s 1 5}$$

$$u^{n+1+a_f} = \left(1 + a_f\right)u^{n+1} - a_f u^n$$

$$v^{n+1+a_f} = \left(1 + a_f\right)v^{n+1} - a_f v^n$$ ……Equation STYLEREF 1 \s 7. SEQ Equation * ARABIC \s 1 4

$$a^{n+1+a_m} = \left(1 + a_m\right)a^{n+1} - a_m a^n$$ ……Equation STYLEREF 1 \s 7. SEQ Equation * ARABIC \s 1 3

7.1.2 *Steady-state calculations*

The steady-state calculation is performed in the initial stages of the simulation without the use of co-simulation by having not to use to the structed coupled conditions. The results of the steady-state simulations are adopted as the initialization for the transient state calculation. For this case, the steady-state simulation was run for 1000 cycles. This is process is preferred before running the transient case because the steady-state solutions can help stabilize the residual before the time accurate calculations begin.

7.1.3 Time accurate calculations

When it is determined that the case under investigation is unsteady in nature, time-accurate computations are used. As mentioned above, the steady-state solution acts as the initialization for the transient state calculation.

7.2 Aspects Regarding the CFD Process

The CFD process for this investigation is described in this chapter. The modelling and discretization processes are covered in the first two subchapters, and the scFLOW process is covered in the final subchapter.

7.2.1 3D CAD Modelling

The Benchmark Supercritical wing is modelled in the SOLIDWORKS software. The description of the model is given in section 5.2. The CAD Model is imported into scFLOW software. The computational domain has been modelled around the wing so as to the simulate the external flow around the wing. The interface surface at the wing is named which becomes the face at which CoSim will exchange data with the Nastran- structural files.

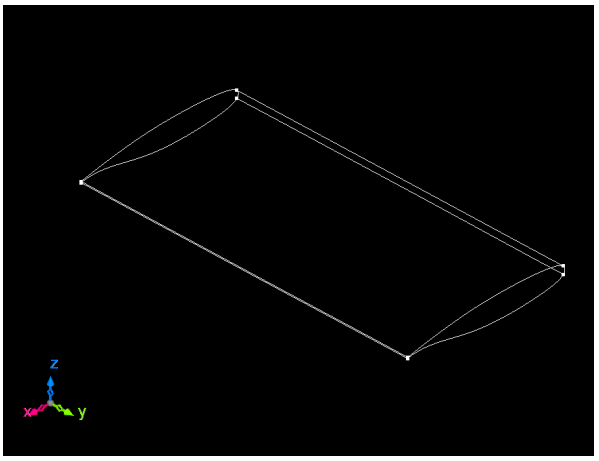

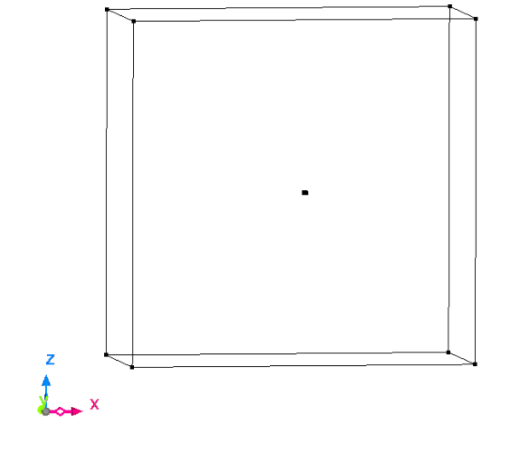

7.2.2 Build Analysis Model

As mentioned in the previous analysis on store separation, the analysis model needs to be build which will create facets on the geometry that will subsequently be the means of mesh generation. The mesher or faceter setting used here is the polyhedral mesher. The facets or the small triangles that are formed during this process are clearly seen in Fig.

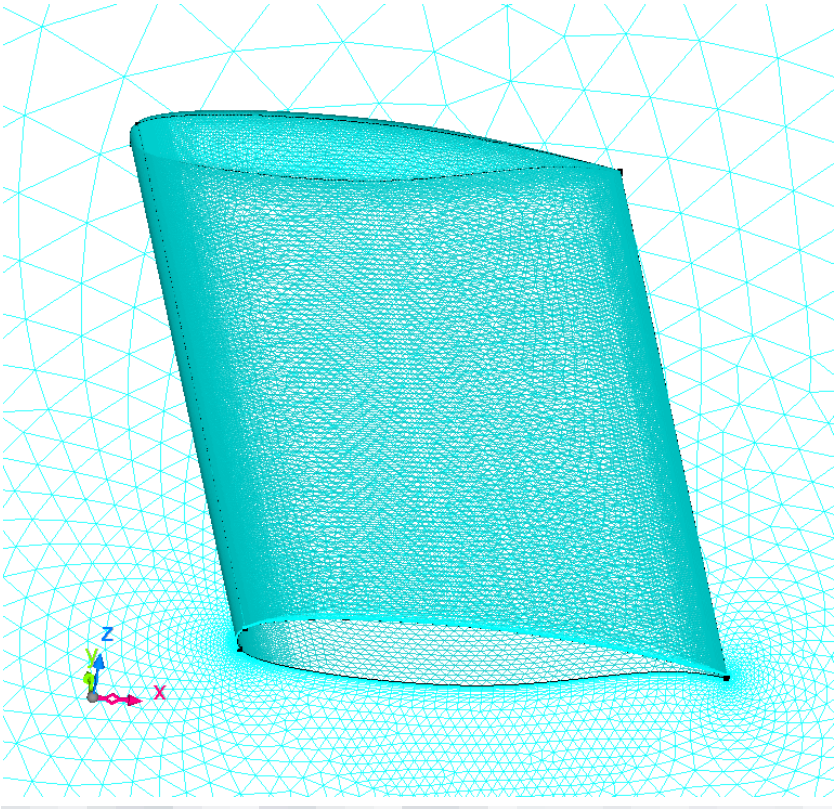

7.2.3 Discretisation

The creation of mesh elements as mentioned before already happens in two stages. The first stage is the octree creation, and the second stage is the polyhedral mesh generation. The general explanation of these terms is already given in section 6.2.3 (a-b). Thus, we can directly move on to the meshing method used.

7.2.3.1 Meshing Method Used

Step 1 Creation of octree

Here the detailed octree parameter setting is used as the fine elements need to be created near the walls of the wing. In a transonic regime, the separation flow and the shock waves exist which needs to be captured accurately. Also, the flow near the walls forms the boundary layer for which we need fine elements near the wall. The maximum and the minimum octant size specified

is 2.048. The octant size specified in different regions is given below in Table 7.1. The value of influence range is also specified here as it enables the software to create finer elements up to a certain range. Say, the influence range is 2, then the finer elements will be created up to 2 layers. Here the wall mentioned by the table stands for Wing.

Table 7.1: The Region Octant size

Region	Size	Influence Range
Wall	0.32	8
Wall Trailing Edge	0.004	2
Wall Leading Edge	0.004	2
Wall tip	0.004	2
Wall Upper surface	0.008	2
Wall Lower surface	0.008	2

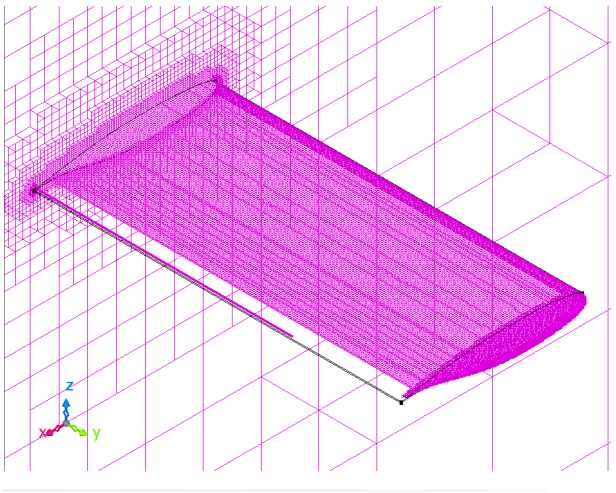

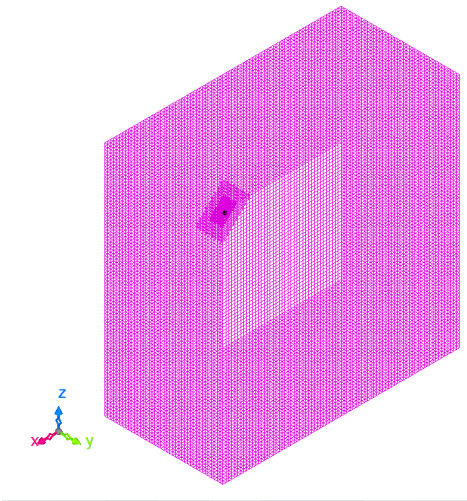

Step 2 Polyhedral Mesh Generation

Following the octree creation, the polyhedral mesh generation takes place. Model shape-oriented mesh is generated with zero number of prism layer

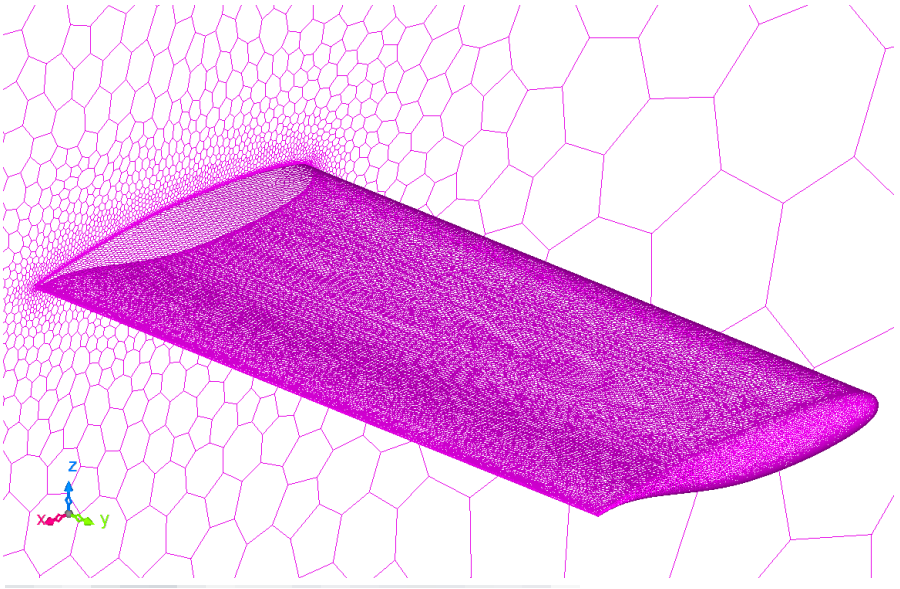

The total number of elements achieved for the mesh is 422147. The element

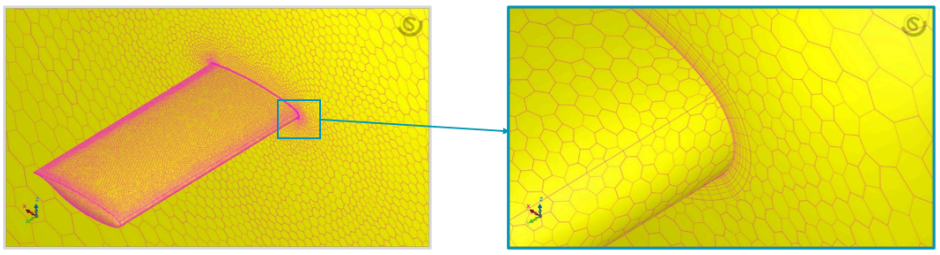

quality was checked which showed zero negative volume check.

7.2.4 CFD Solver Process

7.2.4.1 Material Specification and Registering Regions

The material specified for the fluid domain is the compressible air at 20 degrees Celsius. The wing body is specified as an obstacle. The symmetrical computational domain is considered. The region where the coupling will occur is the wall of the wing, hence it is registered as well. The other regions registered are the inlet, outlet, symmetry and y_{max}. The regions are registered as shown in Figures given below.

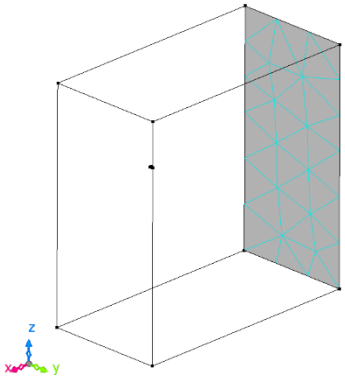

7.8 (a)

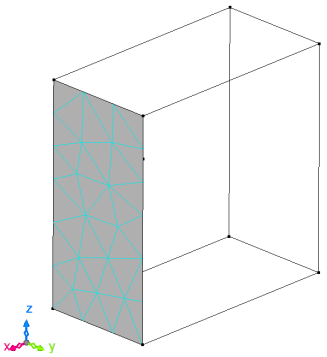

7.8 (b)

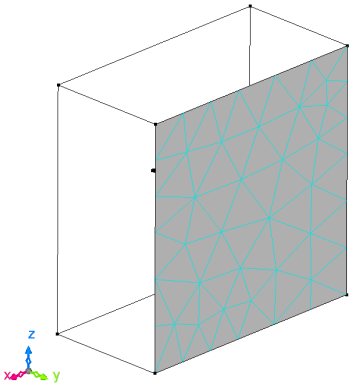

7.8 (c)

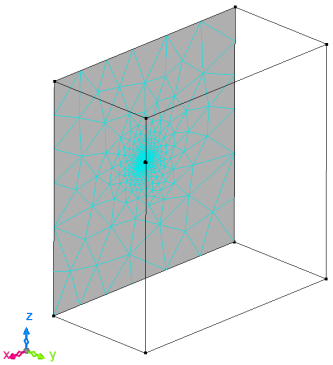

7.8 (d)

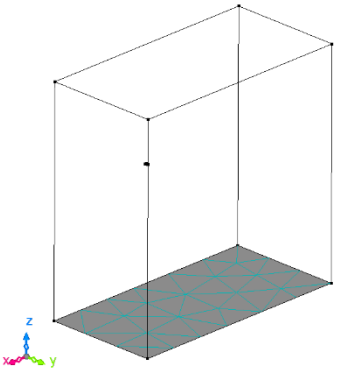

7.8 (e)

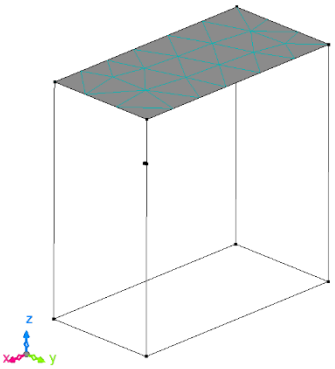

7.8 (f)

7.2.4.2 Analysis and Boundary Conditions

The solver used is the density-based solver. The RANS – SST K-Omega Model has been used for analysis. Wilcox et al. proposed the k-omega model as a two-equation turbulence model, similar to the k-epsilon models. Instead

of solving for turbulence dissipation directly, the dissipation rate per unit turbulence energy with the dimension of frequency [1/s] is considered. This model has the advantage of reproducing near-wall turbulence behavior; it does not require damping functions to obtain a near-wall velocity profile, as was required in the low-Reynolds-number k-epsilon model; and it provides a better estimate of boundary layer separation under adverse pressure gradients. However, the model's strong reliance on boundary conditions like inflow or free-stream turbulence values is a known issue, and it lacks reliability in the outer free-stream layer. In the k-omega model, the eddy viscosity is expressed as follows: [17]

$$\mu_t|_{k-\omega} = \rho\frac{k}{\omega}$$

The k transport equation has the same form as that solved in other low-Re type k-epsilon models, except for the different energy-dissipation expressions shown by Equation 7.7. The omega transport equation is written as follows:

$$\epsilon = C_\mu k\omega.$$

$$\frac{\partial}{\partial t}\rho\omega + \frac{\partial}{\partial x_j}u_j\rho\omega = \frac{\partial}{\partial x_j}\left[\left(\mu + \frac{\mu_t}{\sigma_\omega}\right)\frac{\partial\omega}{\partial x_j}\right] + \frac{\gamma\rho}{\mu_t}G_s - \beta\rho\omega^2$$

.....Equation 7.8

The simulation is run for a total time of 15 seconds. The time step taken here is 0.0002. For Initialisation, the steady-state solutions are used mentioned before.

To predict the flutter dynamics pressure at various Mach numbers, several cases were executed. The flow boundary conditions depend upon the values of the components of velocity calculated which are the V_x and V_z. The temperature values are also calculated as well as the pressure values. Table 7.3 shows all the cases that have been executed. Table 7.3 shows the parameters under consideration used for the calculation of V_x, V_z, Temperature T, and Pressure P. Uniform flow is assumed across the boundaries. The symmetrical boundary condition is applied to the symmetry boundary and the Y_{max}, the top

surface of the computational domain and the bottom as well is subject to the uniform flow condition. No-Slip wall boundary condition is applied to the wall of the wing. The cases executed are to validate the reference data which is the table of Mach number and the Dynamic Pressure values shown in Table 7.2.

Table 7.2: Reference Flutter Dynamic Pressure Values vs. Mach Number

Mach Number	Dynamic Pressure (Pa)
0.70	6300
0.75	5800
0.80	1900
0.83	1000
0.83	2500
0.83	3800
0.85	3800
0.85	11500

With reference to Table 7.2, at each Mach number, 4 cases of flutter were executed with the values of dynamic pressure varying by 50 or 100. The lower side of the reference was performed to check the exact dynamic pressure at which the flutter starts and the higher side of the Dynamic Pressure were checked to see if the flutter still continues beyond the flutter dynamic pressure. The careful investigation was performed at Mach 0.8 at the Transonic Dip occurs at this point. There is a sudden fall in the value of the dynamic pressure that shows the dip. The following tables show the probable cases executed to predict the flutter. The column psf in the tables below defines the Dynamic Pressure Values which are converted from unit Pa to psf. The excel calculator was prepared to calculate the values of Vx, Vz, T and P automatically as shown in Figure below:

Table 7.3: Excel Calculator to calculate Vx, Vz, T and P (Sample Case of Angle of Attack 5 and Mach no. 0.85)

AoA	5						
Mach	0.85						
R	83.66297416	(=a*a/T/γ)					
γ	1.116						
q(psf) – Dynamic Pressure	3800	q(Pa)	1psf=	47.88026	Pa		
μ(slug/ft3-s) - Viscosity	2.59E-07	μ(Pa-s)		5745.631			
Reynolds No.	4.49E+06						
Prandtl Number	6.74E-01						
Chord	0.4064		0.24384	0.48768			
Vx	2.645263E+03						
Vz	2.314305E+02						
V	2.655367E+03						
ρ	5.16E-02						
a	3.123961E+03						
T	1.045235E+05						
p	451302.81						
Cp	804.89551		1slug=	14.5939	kg		
k	1.480934E-02		1ft=	0.3048	m		
			87.913	F	=	304.2128	K
			ref	R	=	84.21945	

The calculator above has been prepared using the basic formulas given below:

Fr ideal gas $P = \rho R T$ .....Equation STYLEREF 1 \s 7. SEQ Equation * ARABIC \s 1 *

Speed of sound in air: $a = sqrt(\gamma RT$ .....Equation STYLEREF 1 \s 7.10)

.....Equation STYLEREF 1 \s 7.11

Mach Number: $M = V/a$

Dynamic Pressure: $q = 0.5\,\rho\, sq(V)$ .....Equation STYLEREF 1 \s 7.12

Reynolds Number: $R_e = \frac{\rho V L}{\mu}$ .....Equation STYLEREF 1 \s 7.13

Prandtl Number: $Pr = Cp\mu/k$ .....Equation STYLEREF 1 \s 7.14

The cases of the dynamic pressure executed has been mentioned in the tables below.

For Mach 0.7:

Table STYLEREF 1 \s 7. SEQ Table * ARABIC \s 1 4: Prediction table at Mach 0.7

case	M	Dynamic Pressure (Pa)	psf	Vx	Vz	T	P
1	0.7	6300	131.5781	91.59439	8.013471	184.7803	23041.45
2		6400	133.6667	93.04827	8.140669	190.6929	23407.19
3		6200	129.4896	90.14051	7.886273	178.9608	22675.72
4		6250	130.5339	94.50215	8.267867	196.6986	23772.93

For Mach 0.75:

Table STYLEREF 1 \s 7. SEQ Table * ARABIC \s 1 5: Prediction table at Mach 0.75

case	M	Dynamic Pressure (Pa)	psf	Vx	Vz	T	P
1	0.75	5800	121.1354	84.32499	7.377481	136.4282	18478.68
2		5900	123.224	85.77887	7.504679	141.1732	18797.28
3		5700	119.0469	82.87111	7.250283	131.7643	18160.08
4		5750	120.0911	83.59805	7.313882	134.0861	18319.38

For Mach 0.8:

Table STYLEREF 1 \s 7. SEQ Table * ARABIC \s 1 6: Prediction table at Mach 0.8

case	M	Dynamic Pressure (Pa)	psf	Vx	Vz	T	P
1	0.8	1900	33	22.97202	2.009791	8.898818	4424.419
2		1700	35.50520778	24.71595	2.162365	10.30122	4760.301
3		1800	37.59374941	26.16983	2.289563	11.54877	5040.318
4		1850	38.63802023	26.89677	2.353162	12.19928	5180.327

The 1700 Pa value of dynamic pressure is highlighted because it the lowest dynamic pressure at Mach 0.8 which is executed to get the Transonic Dip.

For Mach 0.85:

Table STYLEREF 1 \s 7. SEQ Table * ARABIC \s 1 7: Prediction table at Mach 0.85

case	M	Dynamic Pressure (Pa)	psf	Vx	Vz	T	P
1	0.85	3800	79.36458209	55.24735284	4.833517063	45.59310293	9425.63732
2		3700	77.27604046	53.79353077	4.706324114	43.22512953	9177.603726
3		3750	78.32031128	54.52047038	4.769923088	44.40126983	9301.625398
4		5745.96	120	83.53460729	7.30833115	104.2339205	14251.66767

The table 7.4-7.7 shows the case where the dynamic pressure values are taken very low. On the other side, the dynamic pressure values taken of high value is also executed to the get the transonic dip. Table 7.8 shows the values of High Dynamic Pressure executed to capture transonic dip at Mach 0.8.

Table 7.8: High Dynamic Pressure Prediction Table

case	M	Dynamic Pressure (Pa)	psf	Vx	Vz	T	p
1	0.8	4788.3	100	69.61217	6.090276	8.171550E+01	13407.33
2		5745.96	120	83.53461	7.308331	1.176703E+02	16088.80
3		6703.62	140	97.45704	8.526386	1.601624E+02	18770.26

All the cases prepared above in scFLOW is coupled with the Nastran file in MSC CoSim Software. The displacement graph in the x,y and z direction is output to produce the graph which shows the displacement in the z direction. This is because as per the model orientation the flutter should occur in the z direction. The twisting angle and the pitching moment graph is also prepared to check for the divergence in the graph that can predict the onset of flutter.

7.2.4.3 Analysis Control

The discretization method used is cell-centred finite volume unstructured polyhedral mesh as mentioned above. The inviscid flux is calculated using the rotated RHLL flux. This is a robust and accurate Reimann solver by combining the high-resolution Roe solver and dissipative but robust HLLE solver. The accuracy of inviscid terms and limiter functions is of second-order. The viscous flux is calculated using the alpha-damping scheme. This scheme evaluates the gradient at a control volume space by using high-frequency damping term with the parameter alpha in addition to the arithmetic mean of elemental gradient. The calculation method of gradient is the weighted least-squares method. The non-linear solver is the implicit-defect correction solver with the residual Jacobian derived exactly from a lower-order discretization with a local pseudo time-step. The time-integration method is the second-order backward differentiation formula.

7.3 Aspects Regarding the CSM Process (Structures)

The Nastran software is used to prepare the structures of the wing as shown in figure given below. The grid points 13, 14 and 15 which is at the leading edge of the wing to the trailing edge of the wing chosen to map the displacement at these points. [37]

The Nastran file is prepared in the format of a .bdf file. It is in the form of text which can be prepared using software like Apex. Nastran does not have its own pre-processor; hence such is the case. Refer to Appendix A. For this thesis, support was taken from the structure specialist to prepare the Nastran file. It involves making grid points at which the equations will be solved. The file prepared for this thesis uses the CQUAD elements. [38]The material is specified with its properties such as the Young's Modulus and Poisson ratio. The element properties and the boundary conditions are specified. The stiffness matrix is solved in Nastran to get the displacement The FEM Model looks like the Figure given below. Since this thesis focuses on the CFD aspect of the problem, the details on the structure side are limited.

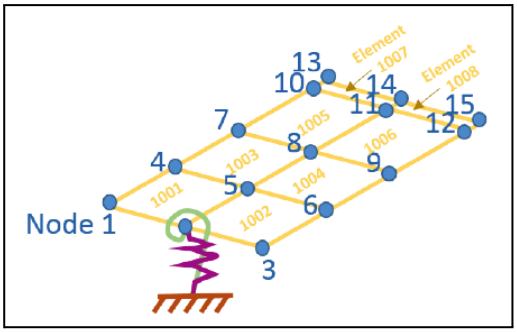

7.4 Aspects Regarding the Cosimulation

Once, the Nastran and the scFLOW files are ready, the structured coupling settings are specified in scFLOW. The two-way coupling happens through the surface where the data mapping region is the wall of the wing. The pressure and velocity data is transferred from scFLOW to Nastran and the displacement vector is received from Nastran to scFLOW. The method of mesh deformation is selected as LDC. [17] RBF (Radial Basis Function) morphing and LDC (Linear Displacement Combination) morphing are the two methods for morphing spatial meshes. The weighted linear combination of the specified

moving surface conditions determines the moving amount of nodes in space in LDC morphing. For the weight, the inverse of the distance to the surface where the moving conditions are specified is used. This distance is calculated before the cycle calculation begins and is not updated during the cycle calculation. The computational cost for each morphing cycle is very low as compared to the RBF Method. LDC morphing is available in both Co-sim and moving conditions. When compared to RBF morphing, mesh morphing has the advantage of taking less time. However, when the amount of deformation from the initial is large, the RBF morphing is more stable. The deformed region is specified as the closed volume which includes the symmetry and the wall regions. Others are all kept as fixed. The time-coupled method used is the Complete Explicit Method. In MSC CoSim, the .bdf files and the .sph files are imported. The grid points 13, 14, and 15 should output the displacement as specified and the CoSim files are generated which is then submitted in Azure HPC for the execution of the simulation.

7.5 Results: Attaining Flutter Dynamic Pressure Points through Comparisons and Testing

7.5.1 Displacements in the Z direction

The data sheet attained through the cosimulation showing the displacements in the z-direction for all the grid points is plotted. The graph shows a Limit Cycle Oscillations at those points where the flutter begins to occur. Thus, for each Mach Number, the flutter dynamic pressure is predicted. For the cases of Mach numbers 0.7, 0.75, 0.8, and 0.85, the graph that is obtained at the low dynamic pressure values is shown in table 7.9.

Table 7.9: The Flutter Dynamic Pressures Values obtained from CoSim

Mach Number	Experimental Dynamic Pressure Values	CFD Dynamic Pressure Values attained
0.7	6300	6250
0.75	5800	5750
0.8	1900	1700
0.85	3800	3800

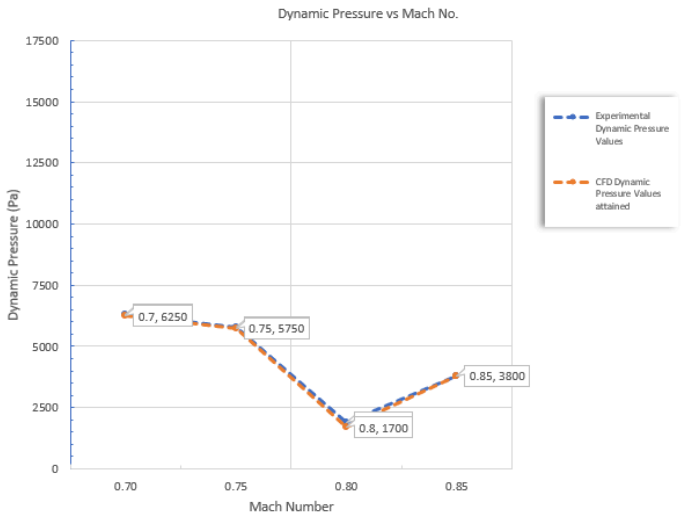

The displacement graphs supporting the above graph on Flutter Dynamic Pressure is given below.

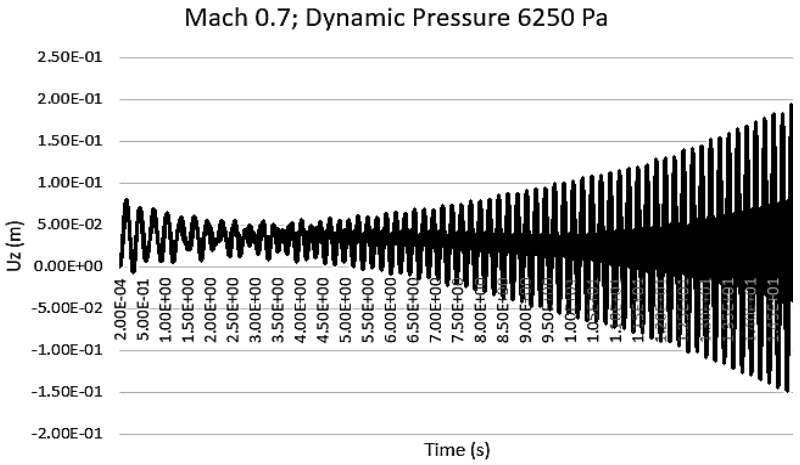

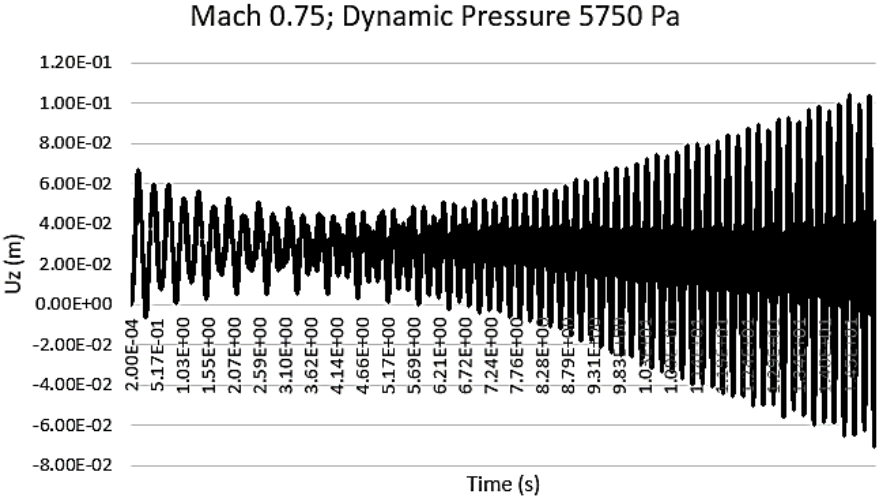

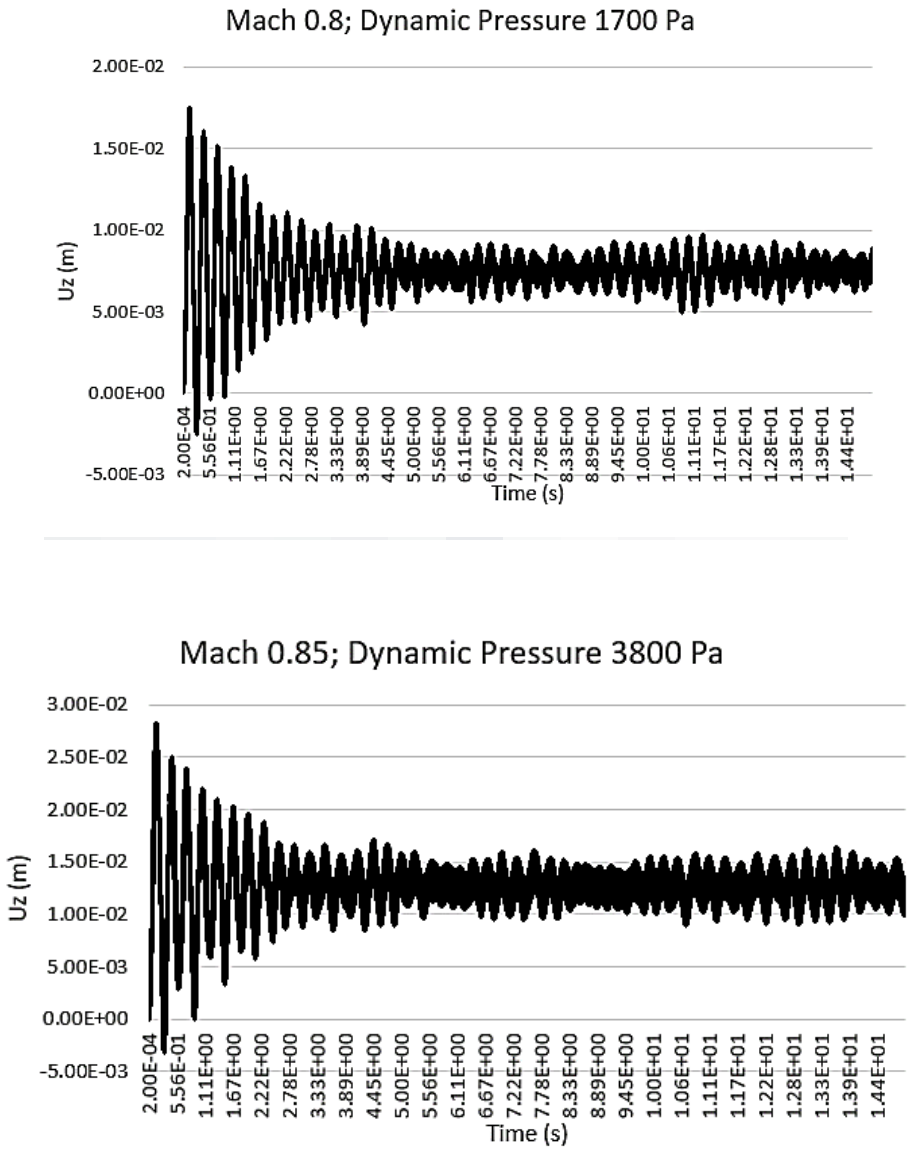

Figure 7.14: Displacement Graph for Mach 0.85 and Flutter Dynamic Pressure 3800 Pa

The graph of displacement for Mach 0.7 and 0.75 shows a huge divergence. This confirms the flutter occurring these points. The graph at Mach 0.8 and 0.85, shows a limit cycle oscillation occurring. The lowest dynamic pressure is 35 psf which can be taken to be the Transonic Dip. This also can predict flutter which means that the wing has started the flutter vibrations is continuously vibrating at that point. However, the question arises of whether the fluctuation in the graph a flutter or just structural vibration is still unknown. In discussion with the AePW III High Angle Working group, this project was able to justify the question, as they still do not have any Wind Tunnel Testing at such low

dynamic pressure values. The validation was done using the reference values provided in the paper “Effect of angle of attack, gas composition and Reynolds number on flutter boundary of benchmark Super-critical wing”. [37] Hence, to study further the dynamic pressure values at which the flutter is occurring, the values at a higher side were taken. This was done specifically for the Transonic Dip, due to the importance of being able to capture the Dip at Mach 0.8.

7.5.2 Transonic Dip at Mach 0.8

The Transonic Dip at Mach 0.8 and Dynamic Pressure Values 120, 140 and 160 psf was performed. The Displacement Graph at Dynamic Pressure showed Limit Cycle Oscillations. By the results of the displacement at nodes 13, 14, and 15 the values were taken further to plot the pitching angle and the pitching moment graph. This case at Angle of Attack 5 degrees where compared to the some conditions at Angle of Attack 0 degrees.

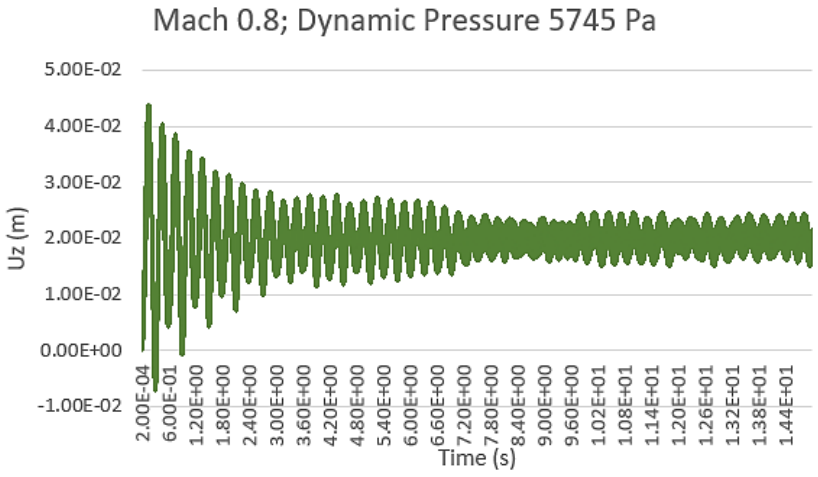

*Figure STYLEREF 1 \s 7. SEQ Figure * ARABIC \s 1 15: Displacement Graph for Mach 0.8 and Flutter Dynamic Pressure 5745 Pa (AoA 5 degrees)*

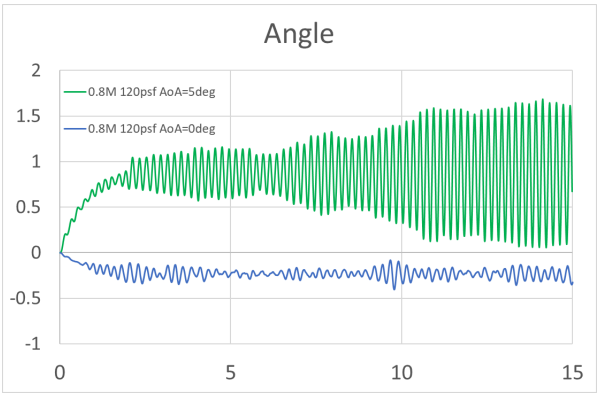

*Figure STYLEREF 1 \s 7. SEQ Figure * ARABIC \s 1 16: Pitching Angle Graph*

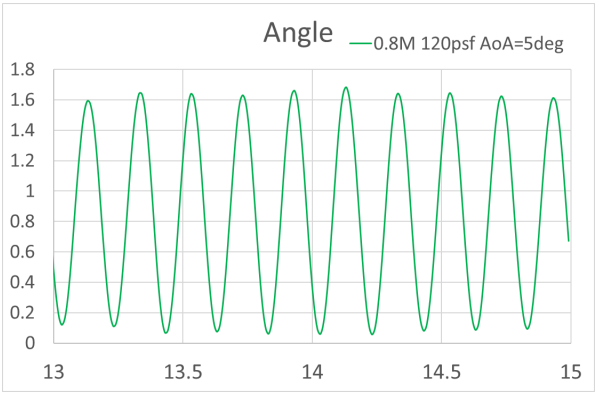

*Figure STYLEREF 1 \s 7. SEQ Figure * ARABIC \s 1 17: Pitching Angle Graph (Clear View)*

At Mach 0.8, Dynamic Pressure 120 psf (5745 Pa), the pitching angle graph showed the limit cycle oscillations to occur. We see the trend in the graph is such that it diverges and then remains constant. Hence, we can conclude that the flutter is occurring in this case.

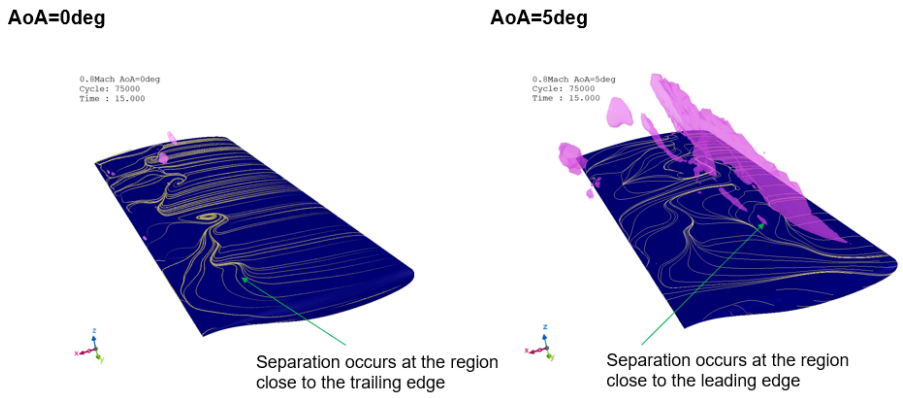

Figure STYLEREF 1 \s 7. SEQ Figure * ARABIC \s 1 18: Separation Contours at Mach 0.8, Dynamic Pressure 120 psf

Also, the Figure shows that at the Angle of Attack of 0 degrees, the separation occurs close to the trailing edge, whereas, for the Angle of Attack of 5 degrees, the separation occurs close to the leading edge. Further analysis was continued to capture the Transonic Dip, for which the cases at dynamic pressure 50 psf, 80 psf, and 90 psf was performed.

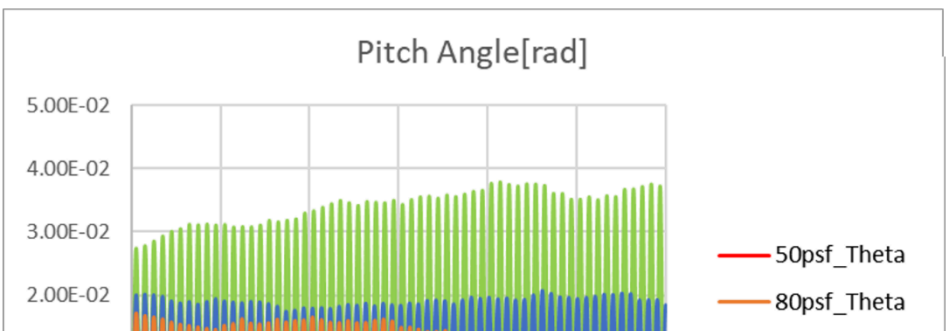

The graph above shows that the flutter boundary for transonic dip occurs around 90 psf.

7.6 Future Work Recommendations:

Detailed Study Can be performed at even lower dynamic pressures at Mach 0.8 at an Angle of Attack of 5 degrees. This can enable us to get the exact point at which the transonic dip is occurring. Further Mesh resolution can be made to finer, to overcome the interference of the shock waves and the flow in the complex transonic regime. Further comparison can also be done with the Wind Tunnel Testing results when it is available with the High Angle Working Group.

Chapter 8: Conclusion

The development of Marketing Content, as well as the development of Benchmarks on CFD problems, clearly helps in understanding the wide range of applications and the industries that are covered under the CFD domain. Industries like Aerospace, Automotive, Electronics, Building, and Architecture have gained through the highly beneficial solutions provided by CFD Cradle. The use of the software enables shortening of development time for products which is major because of many advantages of using the software like automatic mesh generation, reduction in simulation time with highly accurate results, etc.

The project on Store Separation by DSO National Laboratories is in progress. The use of overset mesh and the easy application of 6 DOF parameters in the software-enabled quick pre-processing of the problem. The results of this project will enable us to understand the viscous effects on the store trajectory.

The Co-simulation of Flutter Analysis with the use of MSC Nastran, scFLOW, and MSC CoSim enabled the easy study of Fluid-Structure interaction. The two-way coupling problem involves the transmission of pressure data and displacement data between the two solvers. With the use of Microsoft Azure, the calculation can be done faster.

Chapter 9: Reference

[1] J. Heeg, P. Chwalowski, J. P. Florance, C. D. Wieseman, D. M. Schuster, and B. Perry III, "Overview of the Aeroelastic Prediction Workshop."

[2] H. Ö. Demir, B. T. Selimhocaoğlu, and N. Alemdaroğlu, "CFD Applications in Store Separation Görkem DEMİR."

[3] E. E. Panagiotopoulos and S. D. Kyparissis, "CFD Transonic Store Separation Trajectory Predictions with Comparison to Wind Tunnel Investigations."

[4] Madasamy S, Thilagapathy G, and Arulalagan R, "Investigation of Store Separation and Trajectory of Weapons in Military Aircraft," *International Journal of Scientific & Engineering Research*, vol. 7, no. 2, 2016, [Online]. Available: http://www.ijser.org

[5] K. Jamison, "Optimised transonic store separation analyses using modern design of experiments," *International Aerospace Symposium of South Africa*, pp. 2–3, 2013.

[6] "A. Arabshahi, D. L. Whitfield. 'A Multi-Block Approach to Solving the Three-Dimensional Unsteady Euler Equations about a Wing-Pylon-Store Configuration'. AIAA Paper 89-3401, August 1989

[7] Donegan, "T. L. Donegan, J. H. Fox. 'Analysis of Store Trajectories from Tactical Fighter Aircraft'. AIAA Paper No. 91-0183, In proceedings of the AIAA 29th Aerospace Sciences Meeting, Reno, NV, January 7–10, 1991

[8] K.S. Keen, "K. S. Keen. 'New Approaches to Computational Aircraft/Store Weapons Integration'. AIAA Paper No. 90-0274, In proceedings of the AIAA 28th Aerospace Sciences Meeting, Reno, NV, January 8–11, 1990

[9] "W. L. Sickles, M. J. Rist, C. H. Morgret, S. L. Keeling, K. N. Parthasarathy. 'Separation of the Pegasus XL from an L-1011 Aircraft'. AIAA Paper No. 94-3454, In proceedings of the AIAA Atmospheric Flight Mechanics Conference, August 1–3, 1994.

[10] R. Koomullil, G. Cheng, B. Soni, R. Noack, and N. Prewitt, "Moving-body simulations using overset framework with rigid body dynamics," *Mathematics and Computers in Simulation*, vol. 78, no. 5–6, pp. 618–626, Sep. 2008, doi: 10.1016/J.MATCOM.2008.04.009.

[11] P. Parikh, S. Pirzadeh, and N. T. Frink, "Unstructured grid solutions to a wing/pylon/store configuration," *https://doi.org/10.2514/3.46649*, vol. 31, no. 6, pp. 1291–1296, May 2012, doi: 10.2514/3.46649.

[12] Y. E. Sunay, E. Gülay, and A. Akgül, "Numerical Simulations of Store SeparationTrajectories Using the EGLIN Test," 2013.

[13] "AePW3 | High Angle Working Group." https://nescacademy.nasa.gov/workshops/AePW3/public/wg/highangle (accessed May 14, 2022).

[14] A. Jirásek, M. Dalenbring, and J. Navrátil, “Computational fluid dynamics study of benchmark supercritical wing at flutter condition,” in *AIAA Journal*, 2017, vol. 55, no. 1, pp. 153–160. doi: 10.2514/1.J054916.
[15] “cradle cfd brochure

[17] “scFLOW User’s Guide Analysis Method - 04/Nov/2021.”
[18] “Learning Center.” https://learningcenter-mscemployee.sabacloud.com/Saba/Web_spf/EU2PRD0136/app/content-player?contextid=ctctx000000000219626&assignmentid=cninv000000000004305&subscriptionid=ctnsr000000000006548&launchpoint=LEARNER&regid=regdw000000000062227&signOff=false&spfurl=false&backurl=me%2Flearningeventdetail%2Fcours000000000003239%3FregId%3Dregdw000000000062227%26learnerId%3Demplo000000000013260%26context%3Duser%26returnPage%3DDiscoverPortlet (accessed May 08, 2022).
[19] “MSC Nastran 2022.1 - Online Help (HTML).” https://help.mscsoftware.com/bundle/MSC_Nastran_2022.1/page/MSC_Nastran_main.htm (accessed May 08, 2022).
[20] “E. HEIM, ‘CFD Wing/Pylon/Finned Store Mutual Interference Wind Tunnel Experiment’, Arnold Engineering Development Center, AD-B152 669, September 10-17 1990.
[21] “Store Separation Predictions for Weapon Integration on a Fighter-Type Aircraft
[22] ARNOLD ENGINEERING DEVELOPMENT CENTER ARNOLD AFS TN and E. R. Heim, “CFD Wing/Pylon/Finned Store Mutual Interference Wind Tunnel Experiment,” 1991.
[23] *Verification and validation data for computational unsteady aerodynamics = (Données de vérification et de validation pour l’aérodynamique instationnaire numérique).* Research and Technology Organzation, 2000.
[24] “AePW2.” https://nescacademy.nasa.gov/workshops/AePW2/public/BSCW/publications#publications (accessed May 09, 2022).
[25] “EXPERIMENTAL UNSTEADY PRESSURES AT FLUTTER ON THE SUPERCRITICAL WING BENCHMARK MODEL”.
[26] “AePW3 | High Angle Working Group.” https://nescacademy.nasa.gov/workshops/AePW3/public/wg/highangle (accessed May 09, 2022).
[27] “Arbitrary Lagrangian-Eulerian Method.” http://www.me.sc.edu/research/jzuo/Contents/ALE/ALE_1.htm (accessed May 09, 2022).
[28] “Overset Mesh - Fluid Codes - Ansys Engineering Simulation.” https://fluidcodes.com/software/overset-mesh/ (accessed May 09, 2022).
[29] M. M. Peet, “Spacecraft and Aircraft Dynamics - Lecture 9: 6DOF Equations of Motion”.
[30] “Rizzi, A: Background documentation for software & labwork. Course SD2610 Computational Aerodynamics in Aircraft Design. KTH, Dept. of Aeronautical and Vehicle Engineering, Stockholm, 2010
[31] “Meshing Your Geometry: When to Use the Various Element Types | COMSOL Blog.” https://www.comsol.com/blogs/meshing-your-geometry-various-element-types/ (accessed May 10, 2022).

[32] “Polyhedral mesher.” https://www.cradle-cfd.com/product/scflow/function04.html (accessed May 10, 2022).
[33] E. F. Toro, “Riemann solvers and numerical methods for fluid dynamics: A practical introduction,” *Riemann Solvers and Numerical Methods for Fluid Dynamics: A Practical Introduction*, pp. 1–724, 2009, doi: 10.1007/B79761.
[34] H. K. Versteeg and W. Malalasekera, “An introduction to computational fluid dynamics: the finite volume method, 1995,” *Harlow-Longman Scientific & Technical, London*, vol. M, p. 503, 1996.
[35] “Understanding The k-ε Turbulence Model – All About CFD….” https://cfdisrael.blog/2017/04/25/understanding-the-k-%CE%B5-turbulence-model%EF%81%A5/ (accessed May 11, 2022).
[36] A. A. Osman, A. M. Bayoumy Aly, I. El, O. E. Abdellatif, and E. E. Khallil, “Investigation of the Effect of Grid Size on External Store Separation Trajectory using CFD.”
[37] J. Navrátil, A. Jirásek, P. Hamlington, and L. Col Andrew Lofthouse, “EFFECT OF ANGLE OF ATTACK, GAS COMPOSITION AND REYNOLDS NUMBER ON FLUTTER BOUNDARY OF BENCHMARK SUPER-CRITICAL WING,” 2017.
[38] Hexagon, *MSC Nastran 2022.1*.
[39] “MSCOne - It’s time to explore a smarter way to access simulation software.” https://www.mscsoftware.com/product/mscone (accessed Apr. 27, 2022).
[40] A. Cenko, “Store Separation Lessons Learned (Mistakes Made).”

Chapter 10: Appendix A

NASTRAN File (.bdf)

```
SOL 400
compile NONLIN
alter 'EQUIVX.*OTMNLF.*OTMH.*ALWAYS'
type db,ZUZR12 $
equivx DIT/ZUZR12/-1 $
$
compile IMMDTOUT
alter 'CRDB_OUT.*OESCP.*OESTRCP.*OEFIT.*OES.*OES.*OEF'(1,1)
type db,ZUZR12 $
CRDB_IN GEOM1S,GEOM2S,GEOM3S,EPTS,DYNAMICS//
   'GEOM1'/'GEOM2'/'GEOM3'/'EPT'/'DYNAMIC'/0/0/0 $
CRDB_IN ZUZR12,,,,//
   'DIT'/////0/0/0 $
endalter
CEND
NLOPRM OUTCTRL=(SOLUTION,INTERM)
ECHO = NONE
$  Benchmark Supercritical Wing (BSCW) Faux model$
$  Generated by Jennifer Heeg, 2014 in support of the
$  AePW-2 analysis effort
$
$
$  Note:  a separate .bdf has to be generated to use with the DDF program
$  that maps the mode shapes to the aerodynamic grid.  That .bdf has formatted
$  cards rather than the free format used here.

$  ESE(PLOT) = ALL
$
$
SUBCASE 1
```

```
 STEP 1
  ANALYSIS = NLTRAN
  DISPLACEMENT(PLOT) = ALL
  SPCFORCE(PLOT) = ALL
  NLSTEP = 2
  COSMSEL = 1
BEGIN BULK
PARAM,NLPACK,1
PARAM,LGDISP,1
TABLED1 1
       0.      1.      1.+10   1.      ENDT
TLOAD1  9999999 9999999                 1
NLSTEP  2       15.
       FIXED   75000   100
       MECH            -0.01   0.01
$
$PARAM,  POST,    -1
PARAM,  OGEOM,   NO
PARAM,  AUTOSPC,YES
PARAM,  GRDPNT,   2
$PARAM,  NOFISR,   1
EIGRL         1                 20       0                 MASS
$  May 2, 2014:
$  The published properties of the PAPA mounted wing are not relative to the
30%chord
$  location, but rather relative to the midchord
$  to correct this error, all grid points at the 30% chord are being moved to the
midchord location
$  CORRECTED VERSION:  GRID 2 is at the wing root at the center of
rotation(x/c = 0.5, 16 inch chord --> 8 inches from leading edge)
$  GRID 2 is at the wing root at the center of rotation(x/c = 0.3, 16 inch chord =
4.8 inches from leading edge)
```

```
$  GRId 1000 is the ground point that the springs will attach to
GRID,1000,,0.2032,0.0,0.0,,123456
$  adding grid points to define a rigid wing
$  matrix of 3 points chordwise by 5 points spanwise.
$  chord-wise points are at leading edge, rotational axis and trailing edge
$  spanwise points are at root, 30% 60 % span, 95% span,and wing tip
$1      2       3       4       5       6       7       8       9
GRID    1               0.0000  0.00000 0.00            2
GRID    2               0.2032  0.00000 0.00            1246
GRID    3               0.4064  0.00000 0.00            2
GRID    4               0.0000  0.24384 0.00            2
GRID    5               0.2032  0.24384 0.00            2
GRID    6               0.4064  0.24384 0.00            2
GRID    7               0.0000  0.48768 0.00            2
GRID    8               0.2032  0.48768 0.00            2
GRID    9               0.4064  0.48768 0.00            2
GRID    10              0.0000  0.77216 0.00            2
GRID    11              0.2032  0.77216 0.00            2
GRID    12              0.4064  0.77216 0.00            2
GRID    13              0.0000  0.81280 0.00            2
GRID    14              0.2032  0.81280 0.00            2
GRID    15              0.4064  0.81280 0.00            2
CQUAD4  3001    3000    1       2       5       4
CQUAD4  3002    3000    2       3       6       5
CQUAD4  3003    3000    4       5       8       7
CQUAD4  3004    3000    5       6       9       8
CQUAD4  3005    3000    7       8       11      10
CQUAD4  3006    3000    8       9       12      11
CQUAD4  3007    3000    10      11      14      13
CQUAD4  3008    3000    11      12      15      14
PSHELL  3000    3000    1.0     3000            3000
$  celas1 1000 is the vertical displacement linear spring
```

```
$  celas1 1001 is the torsional rotational linear spring
CELAS1  1000    1000    2       3       1000    3
CELAS1  1001    1001    2       5       1000    5
$1      2       3       4       5       6       7       8       9
PELAS   1000    38484.11
PELAS   1001    4018.643
$  leading edge points
CONM2   4000    1               6.252027
CONM2   4004    4               6.252027
CONM2   4007    7               6.252027
CONM2   4010    10              6.252027
CONM2   4013    13              6.252027
$  rotation axis points
$1      2       3       4       5       6       7       8       9       10
CONM2   4002    2               5.078677                        +3000
+3000               1.183629
CONM2   4008    8               5.078677
CONM2   4005    5               5.078677
CONM2   4011    11              5.078677
CONM2   4014    14              5.078677
$
$  trailing edge points
CONM2   4003    3               6.252027
CONM2   4006    6               6.252027
CONM2   4009    9               6.252027
CONM2   4012    12              6.252027
CONM2   4015    15              6.252027
$
$
$
$  very stiff light material that I may use in future renditions
$MAT1   3000    2.85+19         0.3     1.098-15
```

```
MAT1    3000    2.85+10         0.3     1.098-12
$
$---------- Apended CoSim related info.----------
$
$COSMGRP|- ID -||-TYPE-|
$       |- EID-||-SIDE-||- EID-||-SIDE-||- EID-||-SIDE-||- EID-||-SIDE-|
COSMGRP 1       SURFACE
        3001    1       3002    1       3003    1       3004    1
        3005    1       3006    1       3007    1       3008    1
$
$COSMSEL|- SID-|
$       |CSRVID1
COSMSEL 1
        1
$COSMSRV|CSRVID||-SERV-|
$       |GRPID1|| PHYIN||GRPID2||PHYOUT|
COSMSRV 1       scFLOW
        1       1       1       2
$COSMINP|PHYINID
$       |PHYQUA1|PHYQUA2
COSMINP 1
        FORCE
$COSMOUT|PHYOUTID
$       |PHYQUA1|PHYQUA2
COSMOUT 2
        DISP    VELO    ACCE
$
$       1       2       3       4       5       6       7       8
NLMOPTS SPROPMAP 2
MDLPRM   HDF5    1
enddata
```